UHASSELT
KNOWLEDGE IN ACTION

Maastricht University

Faculteit Geneeskunde en Levenswetenschappen
School voor Levenswetenschappen

Creditcontract transnationale Universiteit Limburg

Masterthesis

ECM, a structure throws cells into chaos - The impact of diseased pulmonary extracellular matrix on adverse basal cell behavior in COPD

Noor Christiaens

Scriptie ingediend tot het behalen van de graad van Creditcontract transnationale Universiteit Limburg

PROMOTOR :

Dr. Niki REYNAERT

Dr. Mieke DENTENER

2016
2017

De transnationale Universiteit Limburg is een uniek samenwerkingsverband van twee universiteiten in twee landen: de Universiteit Hasselt en Maastricht University.

UHASSELT
KNOWLEDGE IN ACTION

www.uhasselt.be
Universiteit Hasselt
Campus Hasselt:
Martelarenlaan 42 | 3500 Hasselt
Campus Diepenbeek:
Agoralaan Gebouw D | 3590 Diepenbeek

UHASSELT
KNOWLEDGE IN ACTION

Maastricht University

Faculteit Geneeskunde en Levenswetenschappen

School voor Levenswetenschappen

Creditcontract transnationale Universiteit Limburg

Masterthesis

ECM, a structure throws cells into chaos - The impact of diseased pulmonary extracellular matrix on adverse basal cell behavior in COPD

Noor Christiaens

Scriptie ingediend tot het behalen van de graad van Creditcontract transnationale Universiteit Limburg

PROMOTOR :

Dr. Niki REYNAERT

Dr. Mieke DENTENER

Maastricht University Leading in Learning!

NUTRIM School of Nutrition and Translational Research

Department of Respiratory Medicine

Faculty of Health, Medicine and Life Sciences

Master Clinical Biomedical Sciences 2016-2017

Dedicated to all the people on this journey.

“Don't think outside the box.

Think like there is no box.”

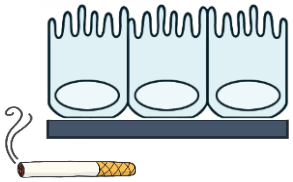

I. Abstract (English)

Background: Basal cells are pulmonary multipotent stem cells and serve to re-establish epithelial integrity after injury. However, in chronic obstructive pulmonary disease (COPD) basal cells seem to accelerate loss of lung function by driving small airways remodelling, including mucous secretory cell hyperplasia and squamous cell metaplasia. Recent evidence suggests that cell behavior strongly relies on the surrounding extracellular matrix (ECM) and its ability to (re)direct intracellular processes. While it is known that both structure and composition of ECM are altered in COPD, it remains to be elucidated whether this compromises cell-matrix signaling, resulting in adverse stem cell behavior and repair.

Methods: To examine the impact of ECM in COPD, we cultured human and murine basal cells on 300µm thick decellularized lung scaffold slices and lung ECM hydrogel derived from SPC-TNFα mice (n=8) versus control littermates (n=8), and assessed differences in cell attachment, proliferation, differentiation, survival, and barrier formation by IHC, IF, and qPCR.

Results: The results show that human and murine basal cells migrate, proliferate, and survive on murine lung scaffold slices for up to 14 days. Differences in recellularization were observed between diseased and non-diseased lung scaffold slices. The mRNA expression of both epithelial and mesenchymal markers seemed to decrease on diseased but increase on healthy matrix over time. Furthermore, we successfully produced lung ECM hydrogel and illustrated that it provides sufficient basis for basal cell survival: human basal cells survived on lung ECM hydrogel for at least 7 days.

Conclusion: Lung scaffold slices and lung ECM hydrogel provide powerful tools *ex vivo* to study cell-matrix interaction in health and disease, supporting viability, proliferation, migration, and site-specific differentiation of basal cells. We demonstrated that basal cells survive on lung ECM hydrogel and that these cells become progressively dysfunctional on transcript level when they are cultured on diseased matrix. Further optimization of the method is needed to confirm the results in human basal cells and human lung tissue.

II. Abstract (Dutch)

Achtergrond: Basale cellen zijn pulmonale multi-potente stamcellen en zijn verantwoordelijk voor het herstel van de epitheliale barrière na long schade. Bij de chronische obstructieve longziekte (COPD) lijken basale cellen het verlies van longfunctie te versnellen door pathologische processen te bevorderen zoals re-modellering van de luchtwegen, hyperplasie van mucus producerende cellen en squameuze cel metaplasie. Recente ontdekkingen suggereren dat het cel gedrag sterk afhankelijk is van de omliggende extracellulaire matrix (ECM) en haar vermogen om intracellulaire processen te reguleren. Hoewel bekend is dat zowel de structuur als de samenstelling van pulmonair ECM veranderd zijn, moet nog worden opgemerkt of dit de signalering tussen cellen en matrix beïnvloed in COPD en resulteert in negatief gedrag van de stamcellen tijdens herstel.

Methoden: Om de impact van ECM in COPD te onderzoeken, werden basale cellen afkomstig van menselijk (PBECs) en muis longweefsel (MTECs) gecultiveerd op 300 µm dikke gedecellulariseerde long slices en long ECM hydrogel afkomstig van SPC-TNFα-muizen (n = 8) versus controle muizen (n = 8). Het doel is het om verschillen in cel hechting, proliferatie, differentiatie, overleving en barrièrevorming te detecteren. Hiervoor werd gebruik gemaakt van technieken zoals IHC, IF en qPCR.

Resultaten: De resultaten tonen aan dat menselijke en muis basale cellen gedurende 14 dagen migreren, prolifereren en overleven op gedecellulariseerde long slices. Verder overleven PBECs minstens 7 dagen op long ECM hydrogel. Verschillen in recellularisatie werden waargenomen tussen zieke (SPC-TNFα) en niet-zieke (controle) long slices. In verloop van tijd, leek de mRNA-expressie van zowel epitheliale als mesenchymale markers te verminderen op SPC-TNFα matrix maar toe te nemen op gezonde controle matrix. Daarnaast werd met succes een long ECM hydrogel geproduceerd dat voldoende basis biedt voor cel overleving: menselijke basale cellen overleefden gedurende ten minste 7 dagen op long ECM hydrogel.

Conclusie: Long slices en long ECM hydrogel bieden krachtige technieken *ex vivo* om cel-matrix interacties te bestuderen. Wij konden aantonen dat basale cellen overleven, prolifereren, migreren, en differentiëren op long slices en o.a. long ECM hydrogel. Verder konden wij aantonen dat basale cellen progressief dysfunctioneel worden op transcriptievlak, wanneer ze op zieke matrix worden gekweekt. Verdere optimalisatie van de methode is nodig om de resultaten in menselijke basale cellen en menselijk longweefsel te bevestigen.

III. List of Abbreviations

A

ATI	Alveolar type I cell
ATII	Alveolar type II cell
AREG	Amphiregulin; epithelial cell growth factor
A549	Human cell line derived from adenocarcinomic human alveolar epithelial cells

B

BC	Basal cell

C

Col-I	Collagen type I; i.a. mesenchymal cell marker
COPD	Chronic obstructive pulmonary disease
CS	Cigarette smoke
CTGF	Connective tissue growth factor; i.a. mesenchymal cell marker
CC10	Clara cell secretory protein; i.a. Club cell marker
Cyto-7	Cytokeratin 7; i.a. epithelial cell marker

E

ECM	Extracellular matrix
E-cad	E-cadherin; i.a. cell adhesion marker
ED-A fibronectin	Extra domain A fibronectin; i.a. mesenchymal cell marker
EGF	Epidermal growth factor
EMT	Epithelial mesenchymal transition

F

FEV	Forced expiration volume
FN	Fibronectin; i.a. mesenchymal cell marker
FOXJ1	Forkhead box J1; transcription factor; i.a. ciliated cell marker
FSP	Fibroblast surface protein; i.a. mesenchymal cell marker
FVC	Forced vital capacity

G

GOLD	Global Initiative of Obstructive Lung Disease

H

HA	Hyaluronan; i.a. mesenchymal cell marker
H&E	Haematoxylin & Eosin; immunohistochemical staining

I

I.a.	Inter alias
IF	Immunofluorescence
IHC	Immunohistochemistry
IPF	Idiopathic pulmonary fibrosis
IVL	Involucrin; i.a. squamous cell marker

K

KC	Keratinocyte chemoattractant; i.a. inflammation marker
Ki67	Cell proliferation marker
kPA	Kilo Pascal; pressure indicator

L

LMP agarose	Low-melting point agarose; embedding medium

M

MTEC	Mouse tracheal epithelial cell

P

PAI1	Plasminogen activator inhibitor-1; i.a. mesenchymal cell marker
P63/TrP63	Transformation related protein 63; i.a. basal cell marker
PBEC	Pulmonary bronchial epithelial cell

Q

qPCR/ RT-PCR	Real-time PCR

S

SHG	Second harmonic generation
SPC	Surfactant protein C; i.a. ATII cell marker
SPC-TNFα mouse	Transgenic mouse model for COPD; overexpression of TNFα in SPC-positive cells

T

TER	Trans-epithelial resistance

Tg+	Transgenic mouse model for COPD; overexpression of TNFα in SPC-positive cells
TGFß	Transforming growth factor ß; i.a. inflammation marker
TNFα	Tumor necrosis factor α; cytokine; i.a. inflammation marker
TTF-1	Thyroid transcription factor-1; i.a. pulmonary epithelial and alveolar cell marker

W

WB	Western blot
WT	Wild-type
WT littermate mouse	Healthy littermates of SPC-TNFα mice

Z

ZO-1	Zona occludens-1

IV. Table of Contents

1. Introduction

1.1. Background

Although COPD is predicted to become the 3rd leading cause of death by 2030, there is poor understanding of the disease pathogenesis. While it is known that both basal cells and the extracellular matrix are deranged in COPD, it is not known whether the associated matrix alterations can induce a diseased phenotype in non-diseased cells. Therefore, this study concentrates on the pulmonary extracellular matrix and its impact on the adverse behavior of basal stem cells in COPD as a driver of the disease pathogenesis.

1.1.1. Chronic obstructive pulmonary disease (COPD)

Chronic obstructive pulmonary disease (COPD) is defined as persistent airflow limitation and is used to describe a combination of two different types of disease: chronic bronchitis and emphysema (1). Chronic bronchitis involves chronic airway inflammation and is associated with increased swelling and mucus production in the airways. Emphysema, on the other hand, refers to irreversible destruction of lung parenchyma and leads to progressive airspace enlargement and loss of lung elasticity in the alveoli (Figure 1) (2). Due to loss of lung elasticity in the alveoli, air gets trapped inside the lungs and in turn enforces airway obstruction as the small airways lose the support of the alveolar structure and start to collapse (3). The extra effort needed to exhale results in shortness of breath, which is also one of the most striking symptoms of COPD. Other symptoms include chronic cough, recurring respiratory infections, and mucus hypersecretion (4).

However, COPD is also associated with extrapulmonary effects that contribute to comorbid conditions such as diabetes, osteoporosis, and skeletal muscle dysfunction (4). The severity of these symptoms and co-morbidities are decisive for the impact of the disease and might vary as not all patients follow the same course of the disease. Based on airflow limitation, COPD severity may be categorized into four different stages, termed GOLD I, II, III, and IV. While stage I is considered mild airflow limitation (FEV1/FVC < 0.70; FEV1 ≥ 80%), stage IV is considered very severe (FEV1/FVC < 0.70; FEV1 < 30% or FEV1 < 50% predicted plus the presence of chronic respiratory failure) (4). Although COPD cannot be cured at any of those stages, it is possible to slow down the disease progression using the appropriate treatment options i.e. anti-inflammatory corticosteroids in combination with bronchodilators. However, in its final stages, the only treatment option remains lung transplantation (5) which is limiting considering the shortage of donor organs and immune reactivity.

To prevent COPD in the first place, it is important to identify the most important risk factors. Although COPD has many causes, cigarette smoke is by far the most common and preventable predisposing factor for developing COPD (1, 4). The inhalation of cigarette smoke is noxious, and has been shown to increase the production of reactive oxygen species in COPD patients (6). In addition, cigarette smoke has been proven to adversely affect the innate immune system, by increasing the number of inflammatory cells, and to cause phenotypical and structural remodelling in the airways, lung parenchyma, and the surrounding extracellular matrix (7, 8). The most predominant structural changes of the lung epithelial lining develop in the proximal airways and involve mucus cell hyperplasia and squamous cell metaplasia (9). In the peripheral airways and alveoli structural remodelling is primarily characterized by airway wall thickening, fibrosis and emphysema (1). In the long run, structural remodelling is considered both limiting and not fully reversible in patients with COPD. Therefore, new therapies are desperately needed and require more understanding of the disease itself, especially with increasing morbidity and mortality on a global scale (4).

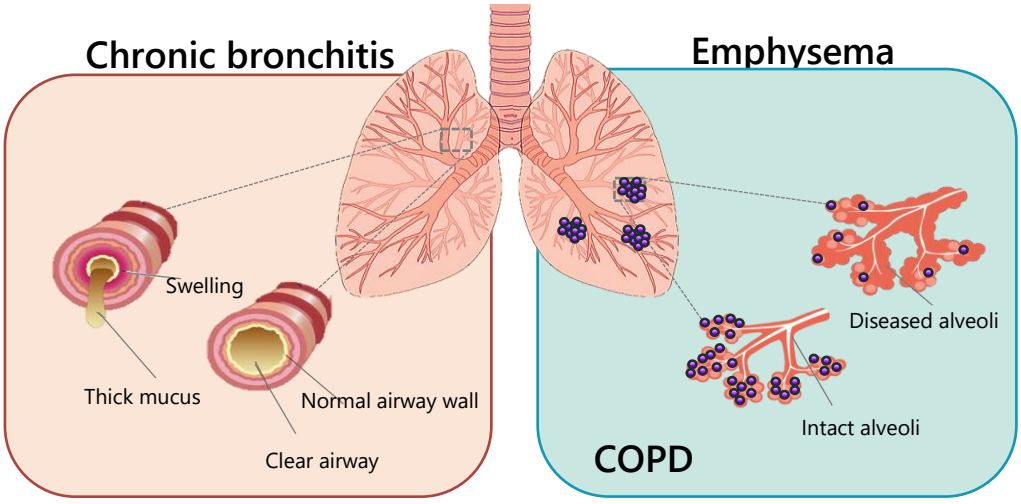

Figure 1. Characteristics of COPD. *COPD is characterized by chronic bronchitis and emphysema. The former includes airway wall thickening, fibrosis, and excessive mucus production. The latter describes the loss of functional lung surface area due to the destruction of alveolar walls and airspace enlargement.*

1.1.2. The pulmonary extracellular matrix (ECM) in health and disease

The extracellular matrix (ECM) is defined as a complex network of secreted proteins that continuously (re)assemble into different and highly specialized structures, including basement membrane and interstitial connective tissue (1). The most abundant matrix proteins constituting the pulmonary ECM are collagen I/III/IV/V, elastin, proteoglycans, fibronectin fibrils, laminin, and glycosaminoglycans such as hyaluronan (10). While collagen fibres provide mechanical strength, elastic fibres serve to maintain lung elasticity and facilitate respiration (1). The other components that constitute the ECM are responsible for supporting overall matrix 3D-structure, water homeostasis, and cell-matrix

interaction(s) (1). In the lung, the ECM ensures efficient gas exchange and acts as a physical barrier to protect the lung parenchyma from the inhaled pathogens (11). Interestingly, pulmonary ECM also plays a role in structural remodelling during lung homeostasis and tissue repair after acute lung injury (10). Due to the exaggerated immune response, the ECM suffers chronic injury and eventually appears to be diseased in COPD (12). The term "diseased" refers to structural and substantial changes, diminishing ECM and tissue function. For instance, changes include the break-down of elastin fibres which are significantly decreased and fragmented in alveolar and small airway walls of COPD patients (1). Degradation of elastin likely results from an increase in neutrophil elastase and contributes to overall loss of alveolar structure. Loss of alveolar structure in turn does not only render the lungs less compliant, but also contributes to small airway remodelling and obstruction (1).

The fractional area of collagen and hyaluronan is increased in patients with COPD and might as well indicate disease severity (1, 13). As both collagen and hyaluronan (HA) are ubiquitously distributed across the ECM, their increased abundance is likely to support airway wall thickening and fibrosis in COPD. Fibrotic matrix remodelling contributes to increased airway obstruction in the small airways and further reduces functional lung surface area, that is needed for efficient gas exchange in the alveoli (14). Depending on its molecular weight, HA might also stimulate the production and release of cytokines, chemokines, and matrix metalloproteinase 12 by macrophages promoting ECM destruction and inflammation (13). In addition, increased levels of HA could also promote angiogenesis and activation of dendritic cells. However, changes do not only involve the ECM itself. As the ECM constantly interacts with cells, the diseased matrix might drive chronic pathological changes in cells as well. Depending on the cell-type and ECM-cell interaction, different cellular processes might be affected.

1.1.3. Bronchial epithelial basal cells (BCs)

Bronchial epithelial basal cells (BCs) are known for their proximity to the basal lamina and are distributed across the epithelial lining of both large and small airways (15). They are interspersed between ciliated, secretory, and neuroendocrine cells. Interestingly, the number of basal cells decreases from proximal to peripheral airways (16) with the consequence that basal cells are completely absent in the alveolar regions (15, 16). In general, basal cells are characterized by the expression of the transcription factor termed transformation related protein 63 (Trp-63) and cytoskeletal protein such as cytokeratin 5. Due to the abundant expression of cytoskeletal, adhesive, and junctional proteins, the main function of BCs was believed to anchor the epithelium to the underlying matrix and to insulate the basement membrane from the external environment (15, 16). More recently however, BCs have been recognized as multipotent stem cells of the lung (16). As

stem cell pool, these cells have the capacity to self-renew, and to regulate both homeostasis and regeneration of the pulmonary epithelium (Figure 2). It has been demonstrated that BCs retain the capability to differentiate towards ciliated-, Club-, and goblet cells, and alveolar type II pneumocytes (ATII) *in vitro* and *in vivo (9, 15, 17)*. The fact that BCs can differentiate towards ATII cells sheds new light on BCs, and might underline their importance in the regeneration and homeostasis of alveolar regions. The capability to differentiate towards ATII cells was previously primarily accredited to Club cells (18). Moreover, ATII cells retain the capability to differentiate towards alveolar type I (ATI) cells (19). While the latter are responsible for mediating efficient gas exchange in the lung, ATII cells primarily serve to reduce surface tension within the alveoli (19). Although there are different subsets of stem- and progenitor-cells in the adult human lung, BCs are the ones proven to reconstitute and therefore repair the complete pulmonary epithelium *in vivo* (20). In addition, BCs show enhanced formation of large differentiated bronchial epithelial cell colonies *in vitro,* when compared to other stem cell cultures of the lung (15, 21).

Despite their benefits and regenerative capacity, BCs have been called the “smoking gun” in COPD by the group of Chrystal (9). Due to persistent inflammation and stress, the pulmonary epithelium suffers chronic epithelial injury in COPD. Each time injury occurs, BCs need to self-renew and, at the same time, generate the appropriate proportions of secretory and ciliated cells (15). Once this balance is disturbed, BCs could contribute, at two extremes, to epithelial cell hypoplasia or epithelial cell hyperplasia. As most COPD patients display the latter, BCs could, at least in theory, be responsible for driving mucous secretory cell hyperplasia and squamous cell metaplasia in COPD (15, 16). In support, a recent study revealed that direct exposure of differentiating BCs to cigarette smoke significantly increased the number of mucus producing cells (MPCs), such as Club and goblet cells, and additionally reduced the number of ciliated cells *in vitro* (22). A decrease in ciliated cells implies less pathogen clearance from the airways in line with increased mucus retention and inflammation. An increase in MPCs on the other hand, contributes to excessive mucus production, secretion, and airway obstruction.

In addition, it has been demonstrated that cigarette smoke increases the exposure of basal cells to stressful mediators such as the epidermal growth factor (EGF) and the EGF-related growth factor amphiregulin (AREG). Both mediators enforce cellular remodelling and further contribute to decreased epithelial resistance in basal cells at air-liquid interface (23). More recently, tumor necrosis factor alpha (TNFα) has been shown to be upregulated in COPD patients. Next to EGF and AREG, TNFα seems to interfere with the transcriptional control and intracellular location of tight junction proteins (24). Overall deregulation of tight junction proteins promotes decreased epithelial resistance and a breakdown of the airway epithelial barrier, which in turn accelerates lung failure in COPD. Pathogens can easily trespass a leaky epithelial barrier and a decreased fluid resorption favours the formation

of alveolar and airway oedema (25). Altogether, this might suggest a direct implication of BCs in COPD. However, the question remains how pathological changes initiate in the first place and how these changes are sustained in the long run, for instance after exposure to cigarette smoke.

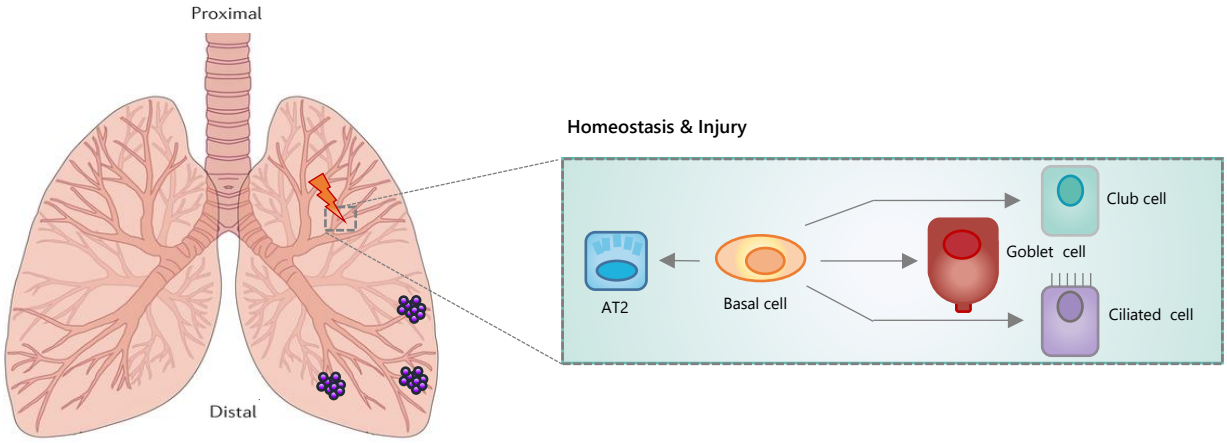

Figure 2.: Basal cell differentiation during homeostasis and injury in the adult human lung. *Basal cells are multipotent stem cells of the lung. Upon injury or during homeostasis, basal cells start to self-renew and differentiate into alveolar type II (ATII) cells, goblet cells, Club cells, and ciliated cells*

1.1.4. The interaction between diseased pulmonary ECM and adverse cell behavior

Previous studies have argued that the adverse behavior of BCs and their progeny results from intrinsic alterations in the transcriptional and regulatory programs of the cells themselves, and that these alterations in turn could lead to pathological auto- and paracrine signaling within the entire stem cell niche (9, 15). Although BCs are indeed able to dictate their own behavior, it should be noted that both cell behavior and cell survival are critically dependent on the extracellular environment (26). In order to respond to changes in their immediate environment, cells must be able to receive, process and integrate signals that originate from outside the cell (27). These extracellular signals may be either mechanical or chemical in nature and include amongst others pressure, shear force and ECM components, neurotransmitters and growth factors respectively (27-29). Once such a signal has activated either intracellular or cell-surface-bound receptors, a signaling cascade is triggered which in turn (in)directly modifies various intracellular processes such as migration, proliferation, differentiation and apoptosis.

The ECM is unique because it can provide both chemical and mechanical stimuli to cells (Figure 3). On the one hand, ECM components can bind (in)directly to cell-surface receptors activating the chemoreceptors located on the cell surface. The indirect interaction is based on the fact that the ECM may function as reservoir for a subset of growth factors, cytokines and chemokines (30). By binding these factors, the ECM renders them insoluble and blocks their bioactivity. On the other hand, the

ECM transmits and receives mechanical forces i.e. fibre stretch and cellular traction forces to and from cells via mechanical strain sensors, also termed mechanoreceptors (31).

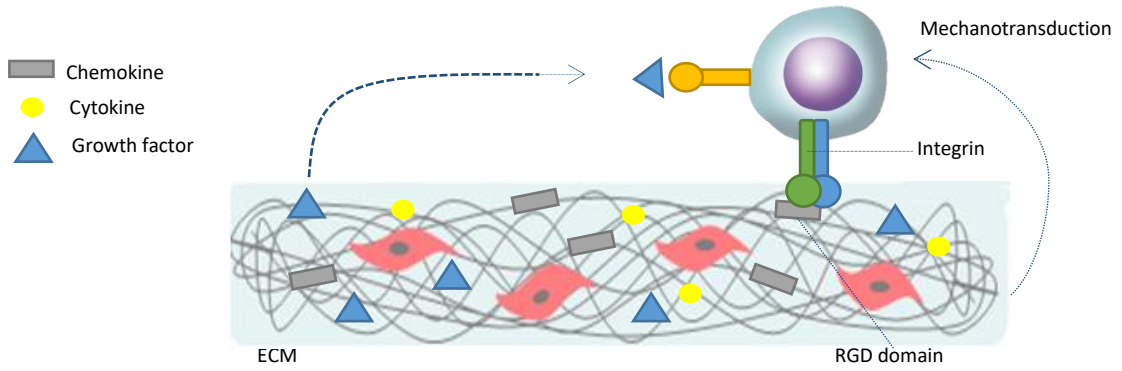

Figure 3: Routes of ECM-cell signaling. *The ECM can interact with cells using a) chemo- or mechanoreceptors that reside on the cell surface, and b) by releasing and storing growth factors, chemokines, and cytokines*

Recent findings indicate that subtle changes in both the structure and composition of the ECM can alter gene expression and cell aggregation of epithelial cells in the lung (32). For instance, a transition from a two-dimensional (2D) to a three-dimensional (3D) matrix seems sufficient to increase the expression of cell differentiation markers and decrease the expression of cell progenitor markers in bronchial epithelial cells, indicating increased cell maturation on 3D versus 2D matrices (32). Moreover, 3D matrices were able to induce 3D-cyst like structures in bronchial epithelial cells that resembled primitive lung structures during early lung development (33).

The fact that the ECM is able to influence cell behavior becomes especially apparent whenever the ECM suffers disease. Although the ECM is known for its dynamic nature, it seems that certain matrix alterations are highly detrimental to cells in their immediate environment. For instance, ECM derived from emphysematous lungs significantly reduces the survival and proliferation of bronchial epithelial cells (34, 35). The reason for this is not yet clear, but it is associated with subtle changes in the ECM that do not sustain long-term survival of epithelial cells.

Furthermore, matrix alterations are associated with epithelial mesenchymal transition (EMT) (1). In this process, the pulmonary epithelial cells lose their polarity and start to differentiate towards mesenchymal cells. This process enforces lung remodelling as it leads to increased depositon of extracellular matrix molecules such as collagen or vimentin.

ECM remodelling is also a hallmark of idiopatic pulmonary fibrosis (IPF) (36). In IPF, it has been demonstrated that the ECM, or more specific the deposition of the matrix component extra domain A (ED-A) fibronectin, is responsible for modulating fibroblast function. Due to increased levels of ED-A fibronectin, fibroblasts get activated and differentiate towards myofibroblasts which display features

of contractile smooth muscle cells (36). While fibroblasts are responsible for maintaining normal tissue architecture, myofibroblasts cause excessive ECM deposition and destroy normal lung architecture (36, 37). Recent evidence also suggests that matrix stiffness seems to play a crucial role in guiding stem cell differentiation and determining lineage commitment. For example, mesenchymal stem cells, prone to differentiate towards the osteogenic cell lineage on stiff matrices (>40kPa), express markers associated with trans-differentiation towards the neuronal lineage when cultured on substrates that are considered soft (<1kPa) (37).

Despite all these findings, it is neither known how nor if a diseased matrix influences basal cell behavior in COPD. Most studies concentrate on pathological processes within the diseased cells themselves and pay little attention to the ECM. Therefore, this study aims to unravel the role of the ECM in disease by providing first proof of principle of adverse cell-matrix signaling in COPD.

We hypothesize that alterations of the pulmonary extracellular matrix render the matrix diseased and result in adverse behavior of basal cells, which in turn diminishes epithelial integrity and drives mucus cell hyperplasia in COPD.

To this end, we use decellularized lung scaffolds, a novel and highly suited 3D-model for studying cell-matrix interaction *ex vivo*. These scaffolds consist of purified ECM and are derived from native lung tissue, providing cells with their natural environment. In contrast to other culture substrates, these scaffolds have the advantage of preserving native ECM composition in both health and disease without disrupting the original 3D-structure of the matrix (38-40). Besides, significant drivers of phenotypic differentiation such as growth factors, chemokines, and cytokines have been sequestered into the 3D-matrix and are retained in the 3D-scaffolds. In scaffold cell culture, these factors are likely to increase cell survival and lineage specification of basal cells when compared to commonly used 2D-cultures (41). Recent evidence already demonstrated that decellularized lung scaffolds support maturation of pulmonary stem cells into functional airway epithelial cells under serum-free conditions, while isolated matrix proteins alone were unable to support such lung lineage commitment (41).

To increase study throughput, decellularized lung scaffolds are sectioned into 300 µm thick lung scaffold slices. These slices are expected to exert the same biological activity as decellularized lung scaffolds, and serve to study basal cell attachment, migration, proliferation, survival, differentiation, and barrier formation over a time course of 14 days (42, 43). Lung scaffold slices derived from SPC-TNFα mice, that overexpress the pro-inflammatory cytokine TNFα in SPC-positive cells, are used to simulate COPD, whereas lung scaffold slices derived from wild-type littermates are used as control. The advantage of using SPC-TNFα mice is that these mice display the two main characteristics of COPD:

chronic bronchitis and emphysema. Moreover, these mice are internally bred in our department and readily characterized for pathological matrix remodelling during COPD (7).

The obtained decellularized lung tissue or tissue slices can also be used to generate lung ECM hydrogel. Lung ECM hydrogel is a solubilized version of the 3D decellularized lung scaffolds. The solubilisation is achieved by mechanically and enzymatically degrading the scaffold. The solubilized and digested matrix components will reassemble spontaneously and form a 3D-architecture *de novo* at 37°C due to the intrinsic self-assembling properties of preserved collagen and elastin recapitulating the complexity of native ECM *in vitro*. In the past, ECM hydrogels have been created from an increasing number of organs and tissues, including the heart, the urinary bladder, nerves, cartilage and adipose tissue (44). More recently, hydrogel has been developed from healthy lung tissue, and was shown to support cell attachment and viability of mesenchymal stem cells (45). In this study, hydrogels are generated from both diseased (SPC-TNFα mice) and control decellularized lung scaffolds (wild-type littermates) to study respective effects of hydrogel on basal cell behavior and function. The aim is to validate lung ECM hydrogel as tool to recapitulate COPD *in vitro*, and to study adverse cell-matrix interaction in both health and disease.

2. Material and Methods

2.1. Cell culture

2.1.1. Mouse tracheal epithelial cells (MTECs)

Tracheal tissue was obtained from C57Bl/6 mice. The trachea was cannulated with PE50 tubing and tied off right before its bifurcation. The open end of the tubing was used to insert a 23Ga needle to fill the trachea with 300ul protease solution, consisting of reduced serum medium Opti-MEM (Gibco, The Netherlands) supplemented with 2µl/ml primocin (Invivogen, The Netherlands), 10µl/ml 100U/ml penicillin and streptomycin (Gibco, the Netherlands) and 0.1% protease Type 14 (Sigma, The Netherlands). Next, the open end of the tubing was sealed using a pair of pre-heated forceps. The filled tracheal tissue was stored overnight in Opti-MEM at 4°C. After 12 hours, the sealed ending was re-opened and the trachea was flushed with Hank's Balanced Salt Solution (HBSS, Gibco, The Netherlands) containing 10% FBS to dislodge the cells. The freshly harvested cells were centrifuged for 5 minutes at 500g and 4°C. Subsequently, the pellet was re-suspended in pre-warmed MTEC culture media consisting of Dulbecco's Modified Eagle Medium Nutrient Mixture F12 (DMEM/F12, Gibco, Germany) supplemented with 50U/ml Penicillin and 50ug/ml Streptomycin, 2mM L-glutamine (Applichem, The Netherlands), 0.2% Primocin (Invivogen, The Netherlands), 20ng/ml Cholera Toxin (Sigma, Germany), 4ug/ml Insulin (Roche, Germany), 5ug/ml Transferrin (Sigma, The Netherlands), 25ug/ml Bovine Pituitary Extract (BPE, Invitrogen, The Netherlands), 10ng/ml Epidermal Growth Factor (EGF, Calbiochem, Germany) and 100nM Dexamethasone (Sigma, The Netherlands). The re-suspended cells were plated on a pre-coated collagen gel, consisting of 18,75% sterile water, 10% 10X Phosphate buffered saline (PBS, BD, the Netherlands), 3.13% 10X MEM, 2.5% 1N NaOH in 3mg/ml collagen (BD, The Netherlands). MTEC medium was changed every 2 days until confluency was reached. Then, MTECs were trypsinized using 0.5% 10X Trypsin with EDTA (Gibco, The Netherlands) for 30 minutes at 37°C. Afterwards, the mixed gel and trypsin solution was centrifuged 5 minutes at 600g and 4°C. The purified pellet was re-suspended in HBSS containing 400µl/ml collagenase (Sigma, The Netherlands) and incubated for up to 2 – 3 hours at 37°C until the collagen fibres were completely dissolved. After centrifugation at 600g and 4°C, the supernatant was removed 2-3 times using MTEC culture medium and MTECs were frozen in freezing media containing 10% FBS (Gibco, The Netherlands) and 5% DMSO (Sigma, Germany) in MTEC culture media. Prior to all experiments, MTECs were thawed and centrifugated at 600g and 4°C. The supernatant was removed and the pellet was dissolved in MTEC media. Cells were plated upon a collagen gel as described above and passaged until ready for recellularization (see 2.2.1.2.).

2.1.2. Pulmonary bronchial epithelial cells (PBECs)

Pulmonary bronchial epithelial cells (PBECs) were isolated from bronchus rings obtained from non-COPD donors undergoing tumor resection surgery (MPTC #2010-019, PLUC facility, MUMC+, Maastricht, The Netherlands). The isolated human bronchial tissue was washed with Hank's Balanced Salt Solution (HBSS, GIBCO®, Thermofisher, Germany) supplemented with 1% 100U/ml Penicillin and Streptomycin (Pen/Strep, Gibco, The Netherlands) and 0.2% mycoplasma elimination reagent (MycoZap, Lonza, Germany). In a second step, the tissue samples were incubated with 1X Protease XIV (Sigma, The Netherlands) diluted in HBSS supplemented with 1% Pen/Strep and 0.2% MycoZap (HBSS+) for 2 hours in 5% CO2 humidified air at 37°C. After a wash with fresh HBSS+, the tissue was gently scraped using rounded forceps to loosen the cells. The obtained cell suspension was centrifuged twice for 5 minutes at 500g at RT, while the supernatant was removed and replaced by first fresh HBSS+, and second complete Keratinocyte Serum Free Medium (KSFM, Invitrogen, Germany) supplemented with 0.2ng/ml EGF, 0.025 mg/ml bovine pituitary extract (BPE, Invitrogen, The Netherlands), 1mM isoproterenol (Sigma, Germany), 1% Pen/Strep and 0.2% MycoZap. After reaching 80-90% confluency in 5% CO2 humidified air at 37°C, pBECs were washed with HBSS+, trypsinized using 2:1 soft trypsin (Thermofisher, The Netherlands) and soft trypsin inhibitor (SBTI, Thermofisher, The Netherlands), and centrifuged for 5 minutes at 500g at RT. The supernatant was removed and cells were re-suspended in freezing medium consisting of KFSM supplemented with 10% DMSO (Sigma, Invitrogen, Germany) and 0.3 mg/ml BPE. Next, cells were stored at -80°C and transferred to LN2 until ready for use. After removal of the freezing media, PBECs were thawed, characterized (Supplementary protocol 1, Supplementary figure 1), and re-suspended in BEGM depending on the number of cells needed for the experiment. Media was replaced ever 2 to 3 days.

2.2. Lung tissue

2.2.1. Mouse lung tissue

Mouse lungs were derived from 8-, 25-, and 39-week-old SPC-TNFα mice (n=9), that overexpress the tumor necrosis factor α (TNFα) in surfactant protein C (SPC) positive cells, and control littermates (n=8). All mice were internally bred and sacrificed in our department.

2.2.1.1. Decellularization

Mouse lungs were decellularized using a 3-day perfusion based decellularization protocol (Supplementary figure 2). All detergents were instilled through both the trachea and the right ventricle of the heart. On day 1, the lungs were rinsed 3x with 5ml DI solution, containing 5X Pen/Strep in de-ionized (DI) water. After a single instillation of 3ml Triton solution, containing 0.1% Triton X-100 solution (AppliChem, Germany) and 5X Pen/Strep in DI water, the lungs were fully incubated in Triton

solution for 24 hours at 4°C. On day 2, the lungs were removed from the Triton solution and rinsed 3x with 5ml DI solution, as described for day 1. Next, 3 mL of 2% sodium deoxycholate diluted in DI water (SDC, Sigma Aldrich, The Netherlands) was instilled and the lungs were fully incubated in SDC solution for 24 hours at 4°C. On day 3, the lungs were removed from the SDC solution and rinsed 3x using 5ml DI solution. Afterwards, the lungs were rinsed and incubated in sodium-chloride (NaCl) solution containing 5,8% 1M NaCl (AppliChem, The Netherlands) and 5X Pen/Strep solubilized in DI water. After incubation for 1 hour at room temperature (RT), the lungs were rinsed with DI solution as described for day 1 and 2. Subsequently, the lungs were instilled with 3ml DNase solution containing 30µg/mL porcine pancreatic DNase (Sigma DN25 – 552 U/mg, Sigma Aldrich, The Netherlands), 1.3mM MgSO4 (Fluka, Sigma Aldrich, The Netherlands), 2mM CaCl2 (Sigma Aldrich, The Netherlands) and 5X Pen/Strep in DI water. After 1 hour of incubation in DNase solution at RT, the lungs were rinsed 3x with 5ml PBS solution. As soon as the decellularized lungs were fully submerged in PBS solution, they were stored at 4°C until ready to use.

2.2.1.2. Generation and recellularization of lung scaffold slices

Heart and residual adipose tissue were removed from all decellularized lungs. The left main bronchus was tied off using an aneurism-clip (10x1,7mm) in order to use the left and right lobe for different end points, as follows (Supplementary figure 3 – 4).

2.2.1.2.1. Right lung

The right upper lobe was tied off using 5.0 suture thread, frozen in liquid nitrogen and stored at minus 80°C until ready for lung ECM hydrogel generation (see 2.7.). The remaining middle and lower right lobe were first inflated using PBS solution to assess the appropriate volume needed for subsequent lobe filling, and were then submerged in pre-warmed PBS solution, and placed upon a pre-heated metal block to maintain a steady temperature at 37°C. Next, middle and lower right lobe were inflated with 3% low-melting point (LMP) agarose (Sigma, The Netherlands) that was solubilized in pre-heated HBSS. The tubing was used to access the trachea using a 2ml syringe. The agarose solution was instilled until the lobes were completely inflated. Next, the re-filled lobes were cut quickly, submerged in ice cold PBS solution, and placed on ice for 30 minutes. Afterwards, the re-filled lobes were stored in PBS solution at 4°C and cut into 300µm thick lung scaffold slices using a Leica VT1000 S vibratome (Leica, the Netherlands). The obtained slices were stored in PBS solution at 4°C. To recellularize individual slices, slices were first submerged in pre-warmed MTEC medium to remove residual PBS solution. The culture media was removed and MTECs were re-suspended in pre-warmed MTEC medium and seeded on top of each slice using a final concentration of $1.5x10^5$ cells/slice. After 2 – 3 hours at 37°C and 5% CO_2, additional MTEC culture medium was added and the recellularized slices were incubated at

37°C and 5% CO_2 for up to 14 days in culture (Supplementary figure 3). MTEC media was changed every 2 to 3 days.

2.2.1.2.2. Left lung

Right after the inflation of the right lung, the trachea was flushed with pre-warmed PBS solution to remove residual agarose from both tubing and trachea. Subsequently, the aneurism-clip was removed from the left main bronchus. The right main bronchus was sealed using 5.0 suture thread. The left lobe was inflated using pre-warmed PBS solution to re-open the left main bronchus and to assess the volume needed for subsequent recellularization of the left lung. Next, the lung was submerged in PBS solution and placed upon a pre-heated metal block to maintain a steady temperature at 37°C. PBECs were re-suspended in BEGM and mixed 1:1 with 3% LMP agarose in HBSS to refill the left lung with a final concentration of $1x10^6$ PBECS/lung. The cell-agarose suspension was instilled in the same manner as described for the agarose instillation in the right lung (see 2.2.1.2.1.). Afterwards, the lung was submerged in cold PBS solution and placed on ice for 30 minutes. Lastly, the lung was cut into 300µm thick lung scaffold slices using the Leica VT1000 S vibratome. Individual slices were quickly transferred to BEGM medium and incubated at 37°C and 5% CO2 for 14 days of culture (Supplementary figure 4). BEGM was changed every 2 to 3 days.

2.2.2. Human lung tissue

Human lung tissue was provided by the PLUC facility (MPTC #2010-019, MUMC+, Maastricht, The Netherlands). All samples were tumor-free lung tissue resections derived from (non)COPD patients and were stored in HBSS+ until ready for use.

2.2.2.1. Decellularization

Human lung tissue was decellularized using an adapted version of the 3-day protocol used for mouse lung decellularization. On day 1, the human samples were incubated 4x 5 minutes in 7ml DI water at 4°C. In between each step of incubation, DI water was replaced as is done for every other solute and incubation step that follows. Next, the samples were incubated 3x 5 minutes in 7ml of Triton solution and subsequently stored in Triton solution at 4°C for 24 hours. On day 2, the samples were removed from the Triton solution. After completion of 4x 5 minutes' incubation in 7ml DI solution, the samples were incubated 3x with 7ml of SDC solution and stored in SDC solution for 24 hours at 4°C. On day 3, the samples were removed from the SDC solution and incubated 4x 5 minutes in 7ml DI solution. Next, the samples were incubated 3x with 7ml NaCl solution and submerged entirely in NaCl solution for 1 hour at RT. Subsequently, the human samples were washed with DI solution as described for day 1 and 2. To remove residual DNA, the samples were incubated 3x 5 minutes in 7ml DNase solution and

transferred to fresh DNase solution. After 1 hour of incubation at RT, the samples were washed 4x 5 minutes with 7ml PBS solution and finally stored in PBS solution at 4°C. Each step of incubation was performed on a rocker plate to ensure constant agitation and sufficient contact between detergent and sample.

2.2.2.2. Generation and recellularization of lung scaffold slices

Decellularized human lung tissue was submerged in 3% LMP agarose containing HBSS. After 5 to 10 minutes, the samples were placed on ice for 30 minutes and stored at 4°C in PBS solution. To generate 300µm thick lung scaffold slices, the samples were either sliced using a tissue chopper or a Krumdieck (TSE Systems, The Netherlands). A subset of decellularized human lung tissue samples was refilled using negative pressure to increase agarose infiltration for Krumdieck slicing. Therefore, these samples were placed in a 50ml syringe together with 3% LMP agarose. Pressure was set on the plunger until the air, trapped inside the sample, was entirely replaced by 3% LMP agarose solution. Another subset of decellularized lung tissue samples were punctured with a syringe, coated with 2.5% sodium alginate (Manugel®, FMC Biopolymer, Philadelphia, PA) in MilliQ and ionically cross-linked with 3% CaCl2 (Sigma Aldrich, The Netherlands). Afterwards, 3% LMP agarose (or methylene blue, Sigma Aldrich, The Netherlands) was instilled using a 2ml syringe.

2.3. RNA extraction and quantification

Individual lung scaffold slices were washed twice in PBS solution, snap frozen in liquid nitrogen and stored at minus 80°C. The frozen tissue samples were then grinded using liquid nitrogen, mortar and pestle. The obtained tissue powder was solubilized in 200ul TRI reagent (Gibco, ther Netherlands) and further fractionated using the Bead-beater (Biospec, Germany) 3x at full speed. In between each run, the homogenates were kept on ice. Next, the samples were incubated for 15 minutes at RT and centrifuged for 5 seconds at 3000 RPM. To separate the homogenates into three different phases (RNA, DNA, and organic phase), 20µl 1-broom-3-chloor-propaan (BCP, Sigma,The Netherlands) was added and the homogenates were centrifuged for 15 minutes at 12000 RPM and 4°C. The upper layer, containing RNA, was transferred to a new 1.5ml Eppendorf tube/ sample and 0.1ul glycogen (Invitrogen, Germany) was added. The samples were mixed gently and centrifuged for 15 seconds at 12000 RPM. To precipitate the RNA, 0.1ml/sample isopropanol (Sigma, The Netherlands) was added and the samples were incubated for 30 minutes at RT. After 15 minutes' centrifugation at 12000 RPM and 4°C, isopropanol was removed and the pellets were washed with 0.2ml 75% ethanol (Mol.Bio, Germany) twice. The pellets were then dried for 10 minutes at 55°C to evaporate residual ethanol, and dissolved in 20ul RNA storage solution (Ambion, The Netherlands). After solubilisation, the samples were incubated at 55°C for another two minutes. To quantify the amount of RNA/sample, the

samples were vortexed, centrifuged at 10000 RPM for 5 seconds, and measured using NanoDrop. Additionally, the DNA phase was transferred to a new 1.5ml Eppendorf tube/sample, stored at minus 80°C and used as positive control during DNA quantification and visualization (see 2.6.).

2.4. cDNA synthesis and qPCR

Extracted RNA was reverse transcribed to cDNA using the transcriptor cDNA syntheis kit (Roche, Germany). Therefore, 400ng RNA/sample was diluted in 12µl nuclease and RNase free water (Invitrogen, the Netherlands). Next, 1µl/sample oligo-dT primer was added. The samples were mixed gently, and centrifuged for 5 seconds at 12000 RPM at 4°C. Afterwards, the samples were incubated at 65°C for 10 minutes to denature the RNA/primer mixture. Then, the samples were placed on ice and a reverse transcription (RT) mastermix was added, containing 4µl reaction buffer, 2ul dNTPs, 0.5ul protector, and 0.5µl Reverse transcriptase per sample. To start the cDNA synthesis, 7µl/sample of the RT-mastermix was added. The samples were mixed gently and centrifuged for 5 seconds at 3000 RPM at 4°C. To activate the reverse transcriptase, the samples were incubated for 60 minutes at 50°C. To denature the RT-enzyme, the samples were incubated for 5 minutes at 85°C. The obtained cDNA was centrifuged for 15 seconds at 3000 RPM and 4°C, and stored at minus 20°C until ready for qPCR analysis (Supplementary protocol 2).

2.5. Immunohistochemistry

Lung scaffold slices were washed twice in 1xPBS solution and fixed in 4% PFA at RT for 30 minutes. Afterwards, single slices were placed in 1xPBS solution, processed for paraffin embedding using the HIT at the department of pathology, paraffin embedded and cut at a thickness of 5µm using the microtome (Leica, Germany). Subsequently, sections were stained for H&E, collagen, TTF-1, and P63.

2.5.1. H&E

The sections were placed for 2x 5 minutes in Xylene, 2x 3 minutes in 100% Ethanol, 2x 2 minutes in 96% Ethanol, 2 minutes in 70% Ethanol, 2 minutes in 50% Ethanol to deparaffinise the slices. After 3x dips in distilled water (ddH20), sections were stained for 5 minutes in Haematoxylin (H). The sections were washed for 5 minutes under running tap water and 1x dip ddH20 to stain slices for 3-4 minutes with Eosin (E). After 1x dip in tap water, slices were dehydrated using 4x dips of 50%, 70%, 96% and 100% of Ethanol respectively. Sections were incubated 2x % minutes in Xylene, air-dried and mounted using VectaMount (Vector Laboratories, The Netherlands). All sections were dried at 37°C.

2.5.2. Sirius red collagen staining

The sections were deparaffinised as described for H&E staining. After 10 minutes wash in running tap water and 5 minutes in ddH20, sections were stained for 5 minutes in Haematoxylin. Afterwards, sections were washed for 5 minutes in running tap water and incubated for 5 minutes in 0.2% phosphomolybdic acid solubilized in ddH20. Then, sections were directly incubated in 0.1% picric acid containing 1mg/ml Sirius red. After 2 minutes of incubation in 0.01M HCl, sections were dehydrated as described for H&E staining.

2.5.3. TTF-1

The sections were deparaffinised as described for H&E staining. After 2 minutes of incubation in ddH20, antigen retrieval was performed using 1mM EDTA (pH=8.0) for 10 minutes at 100°C. After a cool-down period of 30 minutes at RT, sections were rinsed 1x5 minutes in Tris Buffered Saline (TBS, pH=7.5) at RT. Next, endogenous peroxidase was blocked for 20 minutes in 0.6% H202 in methanol at RT. To block non-specific binding places, they were incubated for 20 minutes in 5% BSA/TBS at RT. The primary mouse monoclonal anti-TTF-1 antibody (Neomarkers, USA) was 250x diluted in 0.1% BSA/TBS and incubated over night at 4°C. A negative control was provided by incubating one section without a supplemented primary antibody in 0.1% BSA/TBS. Then, all sections were washed 3x in TBS at RT. The secondary rabbit anti-mouse IgG-biotin labelled antibody (Dako, the Netherlands) was diluted 500x in 0.1% BSA/TBS and incubated for 30 minutes at RT. The sections were washed 3x in TBS and incubated for 30 minutes in Streptavidin ABComplex/Horseradish peroxidase (HRP, Cytomation, The Netherlands) 50x diluted in 0.1% Tween/TBS at RT. The sections were washed 3x in TBS and incubated with DAB using 100µl DAB-chromogen per 1ml DAB-substrate buffer at RT. The enzymatic reaction was stopped after 30 minutes with ddH20. To counterstain the cytoplasm, sections were 1x dipped in Eosin, washed for 5 minutes under running tap water, 1x dipped in ddH20 and dehydrated as described for H&E staining. The sections were mounted using Faramount (Dako, The Netherlands). Lastly, all sections were dried at 37°C.

2.5.4. P63

The sections were deparaffinised as described for H&E and TTF-1 staining. After 2 minutes in ddH20, antigen retrieval was performed by incubating the samples in 20x diluted ready-to-use sodium citrate buffer (pH=6.0; Dako, the Netherlands) for 20 minutes at 100°C. After a cool-down period of 20 minutes at RT, sections were rinsed 1x 5 minutes in Tris Buffered Saline (TBS, pH=7.4). Next, non-specific binding places were blocked using 5% BSA/TBS for 1 hour at RT. The primary mouse monoclonal anti-P63 antibody (Santacruz, USA) was 500x diluted in 0.1% BSA/TBS and incubated over night at 4°C. A negative control was provided by incubating one section in 0.1% BSA/TBS without

a supplemented primary antibody. Next, sections were washed 3x in TBS at RT. The secondary rabbit anti-mouse IgG-biotin labelled antibody (Dako, the Netherlands) was diluted 500x in 0.1% BSA/TBS and incubated for 30 minutes at RT. Then, sections were washed 3x in TBS at RT and incubated for 30 minutes in Streptavidin ABComplex/AP (Cytomation, The Netherlands) 200x diluted in 0.1% Tween/TBS. The sections were washed 3x in TBS at RT and incubated with Vector Blue (VectorLabs, the Betherlands) 50x diluted in 0.1M Tris (pH=8.2) for 18 minutes. The reaction was stopped in ddH20. In addition, sections were incubated in nuclear fast red (Vector, the Netherlands) for 3 minutes to stain non-P63 positive cell nuclei. Afterwards, the sections were washed for further 3 minutes under running tap water, 1x dipped in ddH20 and dehydrated as described for H&E staining. The sections were mounted using VectaMount (Bio-connect, The Netherlands) and dried at 37°C.

2.6. Immunofluorescence

Labtek chambers (Thermofisher, The Netherlands) were washed 3x with 1xPBS after removal of culture media. The cells were fixated using 30 minutes 4% PFA at RT. Next, slices were washed 3x with 1xPBS. Then, cells were permeabilized and blocked using 0.1% Triton X-100 in 1% BSA/PBS for 20 minutes. Afterwards, cells were washed 3x with 1xPBS. The primary antibody mouse monoclonal anti-P63 antibody (Santacruz, USA) was 100x diluted in 1% BSA/PBS and incubated over night at 4°C. After 3x wash with 1xPBS, the cells were incubated with the secondary antibody goat anti-mouse Alexa555 (Dako, the Netherlands) 1000x diluted in 1% BSA for 20 minutes in the dark at RT. In between, a subset of non-P63 stained cells was stained for 30 minutes with Phalloidin-Alexa555 (Abcam, The Netherlands) 40x diluted in 1%BSA/PBS. Next, cells were washed 3x in 1xPBS. To visualize all cells, cell nuclei were counterstained using 2.5µl of 200 µg/ml DAPI (Sigma-Aldrich, Germany) per 1ml 1xPBS and left for 5 minutes in the dark at RT. Then, cells were washed 2x with 1xPBS and 1x with ddH20. Sections were then mounted using Faramount (Dako, the Netherlands), dried for 30 minutes at 37°C, and stored at 4°C until ready for imaging.

2.7. Generation and recellularization of lung ECM hydrogel

Decellularized lung scaffold slices were washed twice in 50mM ammonium bicarbonate solution (pH=7.8), snap frozen in liquid nitrogen and freeze-dried using a freeze dryer. The freeze-dried tissue samples were then minced using a dismembrator (Fisher Scientific, The Netherlands). The obtained powder was transferred to new 1.5ml Eppendorf tubes and further digested under constant agitation in 0.01M HCl containing 100 mg pepsin per 1 g lyophilized ECM powder. After 48 hours, the powder digestion was terminated using cold 1N NaOH (1/10 of the volume of the pre-gel solution) and 10X PBS (1/9 of the volume of the pre-gel solution). The pre-hydrogel was diluted in 1xPBS and coated on

individual Labtek chambers (Thermofisher, The Netherlands). Subsequently, the hydrogel was incubated for 3 hours at 37°C and 5% CO2. Residual fluid was removed and PBECs, submerged in complete BEGM, were cultured on top of the thin coating for up to 7 days (Supplementary figure 5). BEGM was replaced every 2 – 3 days.

2.8. Statistical analysis

Statistical analysis was performed using Excel (Microsoft Excel, The Netherlands). A non-paired T-test was performed to compare means between diseased and control conditions. Differences between different time points within one group were assessed using a paired T-test. Data were expressed as mean +SD. A p-value <0.05 was considered statistically significant while a p value $0.1>p<0.05$ was considered a trend.

3. Results

3.1. Decellularization of lungs derived from SPC-TNFα and control littermates

Residual cells or residual genomic material could interfere with the results by eliciting an adverse immune response in the cells of interest and/or contaminating the stem cell pool during recellularization. Therefore, decellularized tissue was collected prior to all experiments and assessed for residual DNA content and residual nuclear material to determine overall decellularization efficacy. All mouse lungs fulfilled the commonly accepted criteria for whole organ decellularization: the decellularized tissue contained <50ng dsDNA/ mg ECM dry weight, <200bp DNA fragment length, and no visible residual cell nuclei after H&E staining (Figure 4).

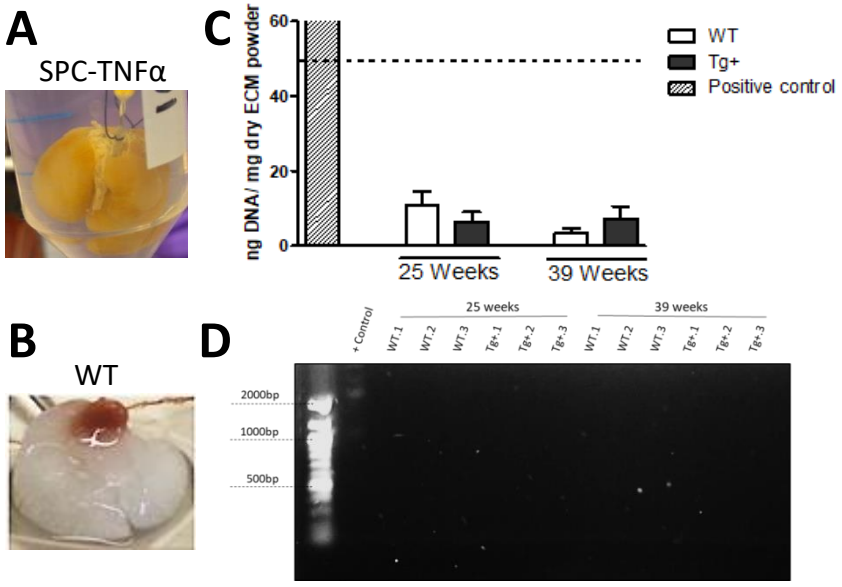

Figure 4. Decellularization efficacy*. The isolated lungs of the 25- and 39-week-old SPC-TNFα mice (A) and control littermates (B) were efficiently decellularized using perfusion based decellularization. The decellularized mouse lungs did contain less than 50 ng dsDNA per mg ECM dry weight (C). No residual DNA fragments were visible after separation on a 0.8% agarose gel indicating <200bp DNA fragment length (D). There was lack of visible nuclear material in tissue sections stained with H&E (E, Figure 4 extended). Black arrows = indicate the slice border; blue arrow = bronchus; Tg+ = SPC-TNFα mouse lung tissue; WT = wild-type littermate mouse lung tissue; positive (+) control = recellularized wild-type littermate mouse lung tissue; bp = base pairs.*

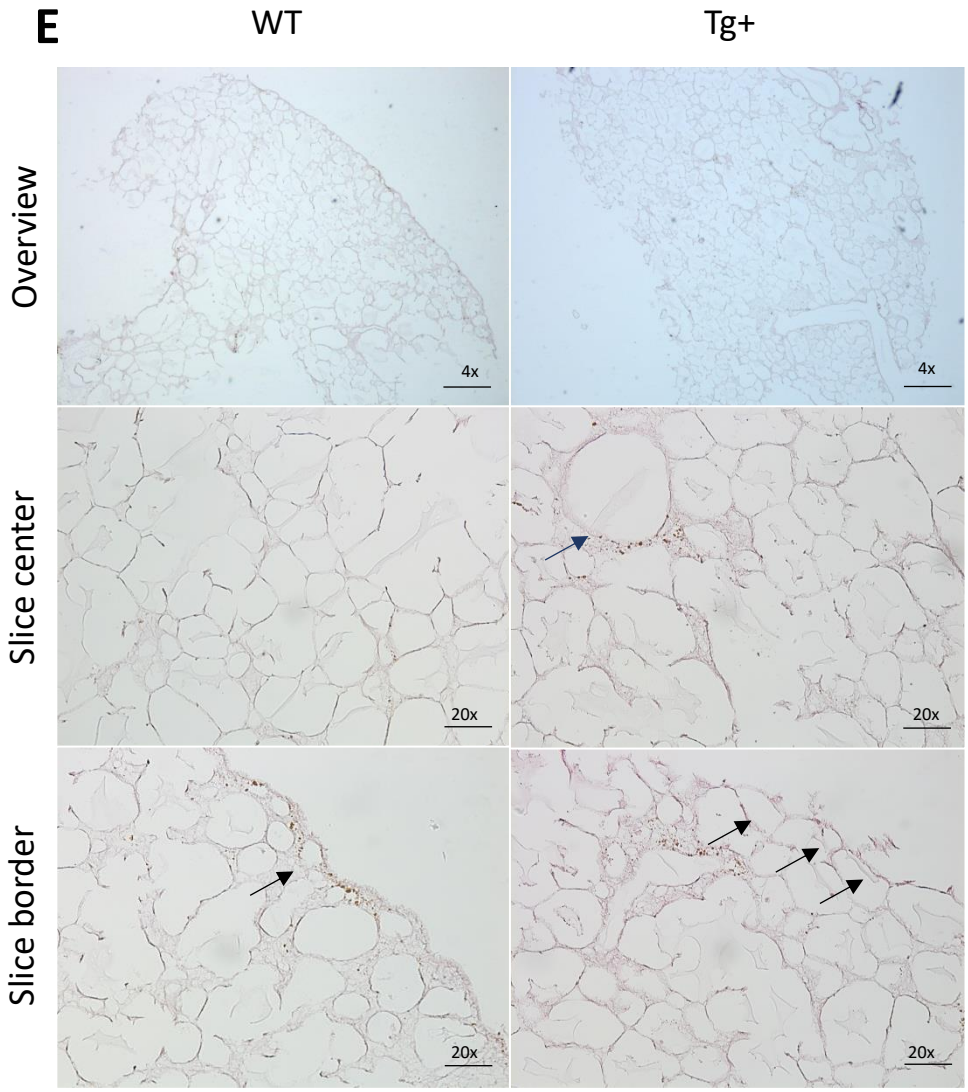

Figure 4 extended. Decellularization efficacy*. The isolated lungs of the 25- and 39-week-old SPC-TNFα mice (A) and control littermates (B) were efficiently decellularized using perfusion based decellularization. The decellularized mouse lungs did contain less than 50 ng dsDNA per mg ECM dry weight (C). No residual DNA fragments were visible after separation on a 0.8% agarose gel indicating <200bp DNA fragment length (D). There was lack of visible nuclear material in tissue sections stained with H&E (E). Black arrows = indicate the slice border; blue arrow = bronchus; Tg+ = SPC-TNFα mouse lung tissue; WT = wild-type littermate mouse lung tissue; positive (+) control = recellularized wild-type littermate mouse lung tissue; bp = base pairs.*

3.2. Collagen and elastin were preserved after decellularization and provided positive control for overall quality of the decellularized material

Decellularization is based on the removal of cells from the tissue or organ of interest using different detergents to induce cell lysis while preserving overall ECM 3D-structure and composition to study cell-matrix interactions *ex vivo*. Therefore, all decellularization detergents are either non- or an-ionic and have been specifically selected for minimal matrix but maximal cell degradation as demonstrated by other research groups (38, 46-48). In this study, we confirmed that the scaffold slices retain major pulmonary ECM components after decellularization and slicing. Therefore, slices were analysed for

relative distribution and overall appearance and aggregation of collagen and elastin fibres using two-photon microscopy and Sirius red collagen staining (Figure 5 - 6).

The two-photon microscopy imaging was based on 1) the auto-immunofluorescent properties of elastin and 2) second harmonic generation (SHG) technology for the visualization of collagen. The obtained images demonstrated that the scaffolds maintain intact collagen and elastin fibres after decellularization (Figure 5). The aggregation of both fibre types resulted in the formation of a highly-interwoven network of collagen and elastin. While alveolar regions seemed to contain more elastin fibres, bronchial regions seemed to contain more collagen fibres lining larger airway structures.

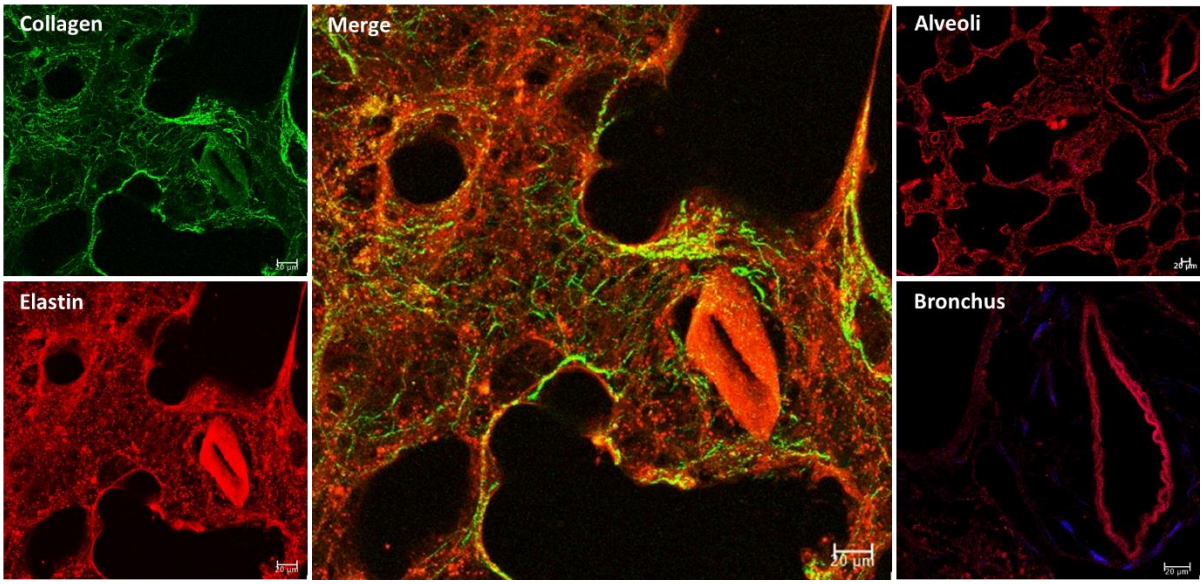

Figure 5. Collagen and elastin are preserved after decellularization and slicing of mouse lung tissue. *Decellularized lung scaffold slices derived from 25-week-old SPC-TNFα mice were analysed using two-photon microscopy and showed intact structures of collagen and elastin fibres. Both collagen (depicted in green and blue) and elastin (depicted in red) resulted in interwoven networks throughout the scaffold. Elastin was localized primarily in alveolar regions and was less present around bronchial tissue in contrast to collagen.*

To compare the relative retention, distribution and abundance of collagen fibres between diseased and WT scaffolds, recellularized WT and Tg+ scaffold slices were stained with Sirius red to visualize collagen fibres and counterstained with Haematoxylin to visualize cell nuclei (Figure 6). While the slice border and the bronchial areas displayed large amounts of collagen, the alveolar regions seemed to contain relatively few collagen fibres under WT conditions. With regards to the relative distributions of cells, it seemed that MTECs and PBECs preferred to repopulate in close association with dense areas of collagen (data not shown). In accordance with the used mouse model, collagen staining showed that the Tg+ lung slices contain higher levels of collagen in the alveolar regions compared to WT controls. As SPC-TNFα mice were used for the generation of Tg+ slices, increased collagen deposition likely indicates fibrotic remodelling within alveolar regions. In agreement, previous studies in our department have demonstrated that SPC-TNFα mice contain a higher fractional area of collagen

in bronchial regions and that collagen deposition occurs in both small airways and alveolar regions of the lung (1). Although the results of this study seem to validate these findings, we did not specifically calculate for fractional area of collagen and elastin fibres or relative cell distribution inside the scaffold slices to confirm the observations.

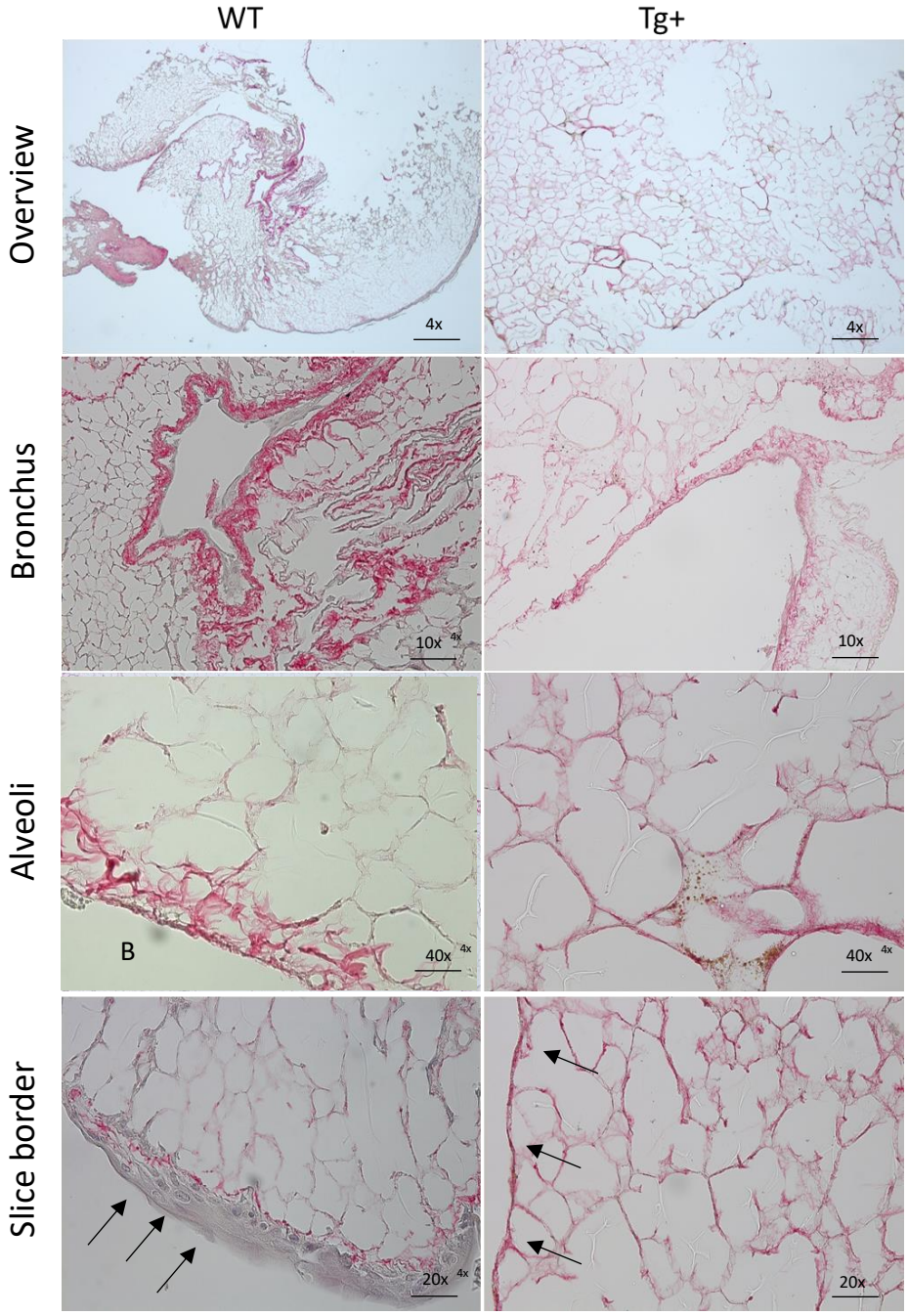

Figure 6. Collagen staining of recellularized lung scaffold slices. *The abundance and relative distribution of collagen fibres was visualized using Sirius red staining. Cell nuclei were counterstained using Haematoxylin. Pictures were depicted at day 7 of MTEC recellularization. In WT, collagen fibres were primarily located around bronchial structures and were less visible in alveolar regions under WT conditons. In SPC-TNFα mouse derived lung scaffold slices, collagen deposition was mostly encountered in bronchial regions of the lung but was also visible in in alveolar regions indicating signs of fibrotic lung remodelling. B = Bronchus. Black arrow = Slice border. Images were taken at 10x, 20x, and 40x magnification.*

3.3. Basal cell recellularization was different between diseased and non-diseased scaffolds

A lot of physiological processes such as cell attachment, proliferation, migration and survival depend on efficient cell-matrix signaling including structural and mechanical support of the ECM. Any disruption of the tightly regulated cell-matrix interaction may promote pathological processes. To study whether the diseased ECM initiates pathological processes in non-diseased basal cells, MTECs and PBECs were cultured on decellularized matrix derived from 25- and 39-week-old SPC-TNFα mice versus control littermates. The recellularized matrix was used for histological assessment at day 7 and 14.

3.3.1. MTECs

Haematoxylin and eosin (H&E) staining showed that MTECs survive on decellularized lung scaffold slices for at least 14 days of culture (Figure 7). However, matrix origin seemed to influence cellular engraftment. While basal cells clustered at the slice border and/or around bronchial structures from WT mice, cells tended to spread more evenly on SPC-TNFα derived lung scaffold slices at day 7 and day 14. In between both time points, cell proliferation seemed to take place as more cells were visible at day 14 compared to day 7. In WT mice, cell proliferation became visible as active cell cluster formation at the slice periphery and/or around bronchial structures. At the slice border, cells seemed to form a non-keratinized cell monolayer. The repopulation of the slice border was further associated with the presence of a diffuse structure around the apical side of the cells. In contrast, there was less cell cluster formation at the slice periphery under diseased conditions. The slice border and bronchial structures were lined by flattened epithelial cells which appeared to form a discontinuous cell monolayer. In Tg+ mice, there was no or reduced deposition of the aforementioned diffuse structure at the apical side of the cells. At repopulated regions of the scaffold, dense yellow particles were observed (Figure 7, indicated with black arrows), which were not or less present in WT mice prior to recellularization and might represent deposition of cell debris on the matrix.

3.3.2. PBECs

Preliminary data had indicated that PBECs grow and survive on decellularized mouse lung tissue for 28 days (data not shown). Therefore, mouse lung tissue was expected to display no or negligible adverse immune reaction towards human epithelial basal cells and to provide sufficient basis for their cell growth. To study the effect of diseased matrix on human pulmonary epithelial cells, PBECs were seeded within both diseased and non-diseased mouse lung scaffolds (Supplementary figure 4 and 5). The advantage of using PBECs is that these cells reflect the natural behavior of human basal cells *ex vivo*. The usage of mouse lung scaffold slices on the other hand allows for controlled experimental settings and conditions such as specific slice thickness and the implementation of SPC-TNFα mice

and wild-type littermates to reduce group-dependent variation. Moreover, mouse lung scaffold slices recapitulate the whole lung structure (including both alveolar and bronchial regions), contrary to human lung tissue slices that are mostly obtained from peripheral tumor resections and therefore contain little bronchial tissue. Besides, human scaffold slices would introduce higher donor-dependent variability between the two test groups. The results illustrate that repopulation of mouse lung scaffold slices using PBECs differed from recellularization using mouse basal cells (MTECs). In contrast to mouse basal cells, PBECs did not form large cell clusters at the slice border or around bronchial regions in neither the WT nor the Tg+ group. There were no obvious increases in the number of cells between day 7 and 14. While PBECs seemed to attach to alveolar and bronchial regions under WT conditions, they seemed to be less able to repopulate these regions under diseased conditions.

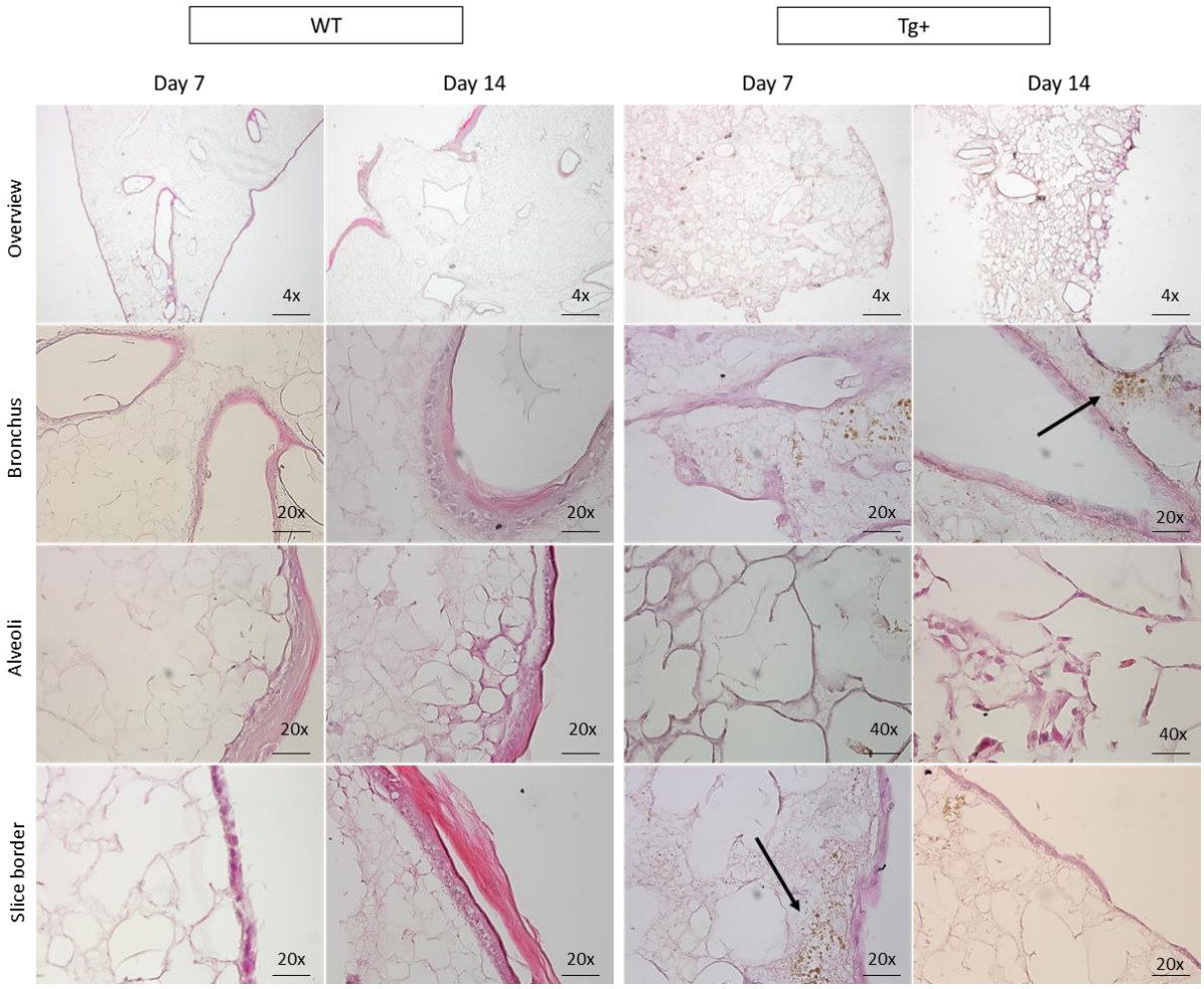

Figure 7. Repopulation of lung scaffold slices using MTECs resulted in differential engraftment of diseased versus control lung tissue. *Mouse lung slices were efficiently recellularized with MTECs. However, while MTECs did cluster at the slice periphery or around bronchial structures in the WT group, they did spread more evenly over the entire scaffold under diseased conditions. Black arrows indicate cell debris that was found in increased amounts on diseased scaffolds. Images were taken at 4x, 10x, 20x, and 40x magnitude respectively.*

3.4. Epithelial barrier formation

The integrity of the airway epithelial barrier is often disrupted in patients with COPD. The tight junction protein Zona occludens-1 (ZO-1) and the cell-cell adhesion molecule E-cadherin play a key role in the maintenance of a functional epithelial lining. Loss or dysfunction of these barrier molecules contributes to chronic inflammation and epithelial mesenchymal transition (EMT). To study whether a diseased matrix decreases the functionality of the epithelial barrier, mRNA expression of ZO-1 and E-cadherin were measured in mouse basal cells. Therefore, MTECs were seeded and cultured on diseased ECM scaffold slices derived from 39-week-old SPC-TNFα mice. Both ZO-1 and E-cadherin expression were assessed at mRNA level. ZO-1 expression tended to be decreased in diseased matrix at day 7. This trend appeared to be consistent as ZO-1 expression remained low after further 7 days of culture in scaffolds derived from SPC-TNFα mice compared to scaffolds derived from WT mice. The mRNA expression of E-cadherin did not differ between scaffolds derived from SPC-TNFα mice versus controls, neither at day 7 nor day 14. However, the mRNA expression of both epithelial barrier markers tended to increase over time in both conditions (Supplementary figure 9).

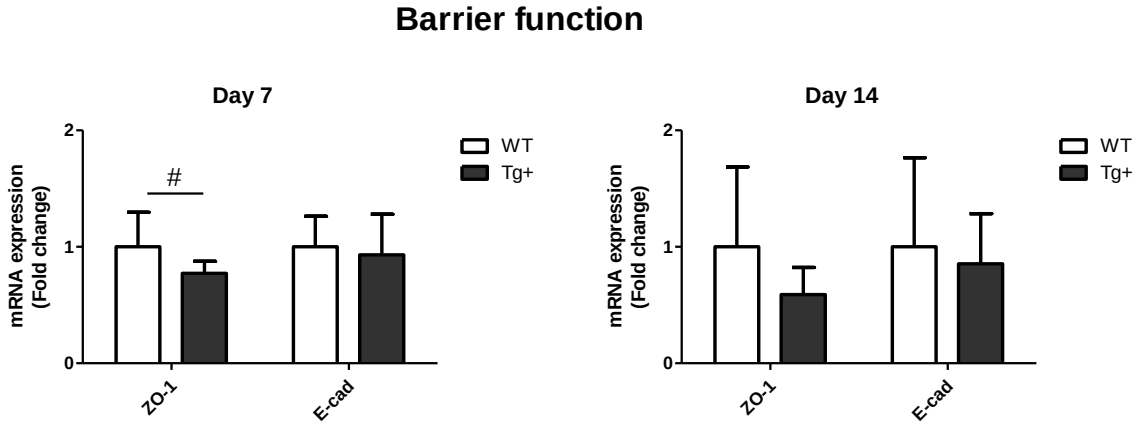

Figure 8. The diseased extracellular matrix might influence the mRNA expression level of junctional proteins. *The mRNA expression of ZO-1 tends to be lower in MTECs cultured on diseased versus control matrix derived from 39-week-old SPC-TNFα mice at day 7 and 14. The expression of E-cadherin remains relatively unchanged on mRNA level and shows little differences between WT and Tg+ culture. The relative mRNA expression was measured using qPCR. Data were corrected for the expression of the housekeeping genes RPLO, YWHAZ, and RPL13A, and are expressed as mean + SD, # indicates 0.1>p>0.05 compared to controls.*

3.5. Differentiation

Pulmonary epithelial cells display adverse behavior in COPD. Although the underlying mechanisms remain unknown, it seems that mucus cell hyperplasia, EMT and squamous cell metaplasia may result, at least in part, from misguided cell differentiation of basal cells which usually proliferate and differentiate after lung injury to replace the damaged cells. To determine if a diseased matrix can trigger pathological changes with regards to basal cell differentiation, we compared the mRNA expression of different epithelial (P63, Cytokeratin-7, SPC, forkhead box J1 (FOXJ1), involucrin (IVL), and Clara cell secretory protein (CC10)) and mesenchymal (plasminogen activator inhibitor-1 (PAI-1), collagen type I (Col-I), connective tissue growth factor (CTGF), fibroblast surface protein (FSP), and fibronectin (FN)) cell markers between MTECs grown on diseased versus MTECs grown on control ECM scaffold slices derived from 39-week-old SPC-TNFα mice (Figure 9A&B).

3.5.1. Epithelial markers

The results illustrate that MTECs which were cultured on diseased matrix show increased expression of epithelial markers at day 7: for instance, mRNA expression of P63, Cytokeratin-7, SPC and FOXJ-1 were higher in the Tg+ group compared to healthy controls (Figure 9A). An exception was seen for CC10: this marker seemed to be down-regulated on diseased matrix at both day 7 and day 14. After prolonged cell culture, MTECs seemed to display a shift within their mRNA expression profile. Despite initial increase, most epithelial marker decrease in the Tg+ group at day 14. Therefore, the initial increase of mRNA expression seemed to be transient. In contrast, the WT group seemed to increase the expression of epithelial markers with prolonged cell culture and showed enhanced expression of epithelial markers at day 14 compared to day 7.

3.5.2. Mesenchymal markers

Mesenchymal markers seemed to display a similar behaviour. The mRNA expression of PAI-1, CTGF, and FSP was higher in the Tg+ group compared to healthy controls at day 7 (Figure 9B). After prolonged cell culture, MTECs seemed to display a shift within their mRNA expression profile comparable with the shift observed for epithelial markers under diseased conditions. Despite an initial increase, the mRNA expression of most mesenchymal markers tended to decrease in the Tg+ group from day 7 to day 14. Especially, the EMT marker CTGF was affected after prolonged cell culture: CTGF was significantly decreased on diseased versus control matrix at day 14. Direct comparison of mRNA expression between both groups suggests that both WT and Tg+ group decrease their overall expression of mesenchymal markers over time. However, not all mesenchymal markers followed the same expression pattern. At day 14, CTGF mRNA expression was significantly upregulated in the WT group and differed significantly from the CTGF expression of the Tg+ group. The mesenchymal marker

PAI-1 and collagen type I showed a significant increase in mRNA expression in the Tg+ group from day 7 to day 14. Another exception was seen for fibronectin which seemed to be down-regulated on diseased matrix at both day 7 and day 14.

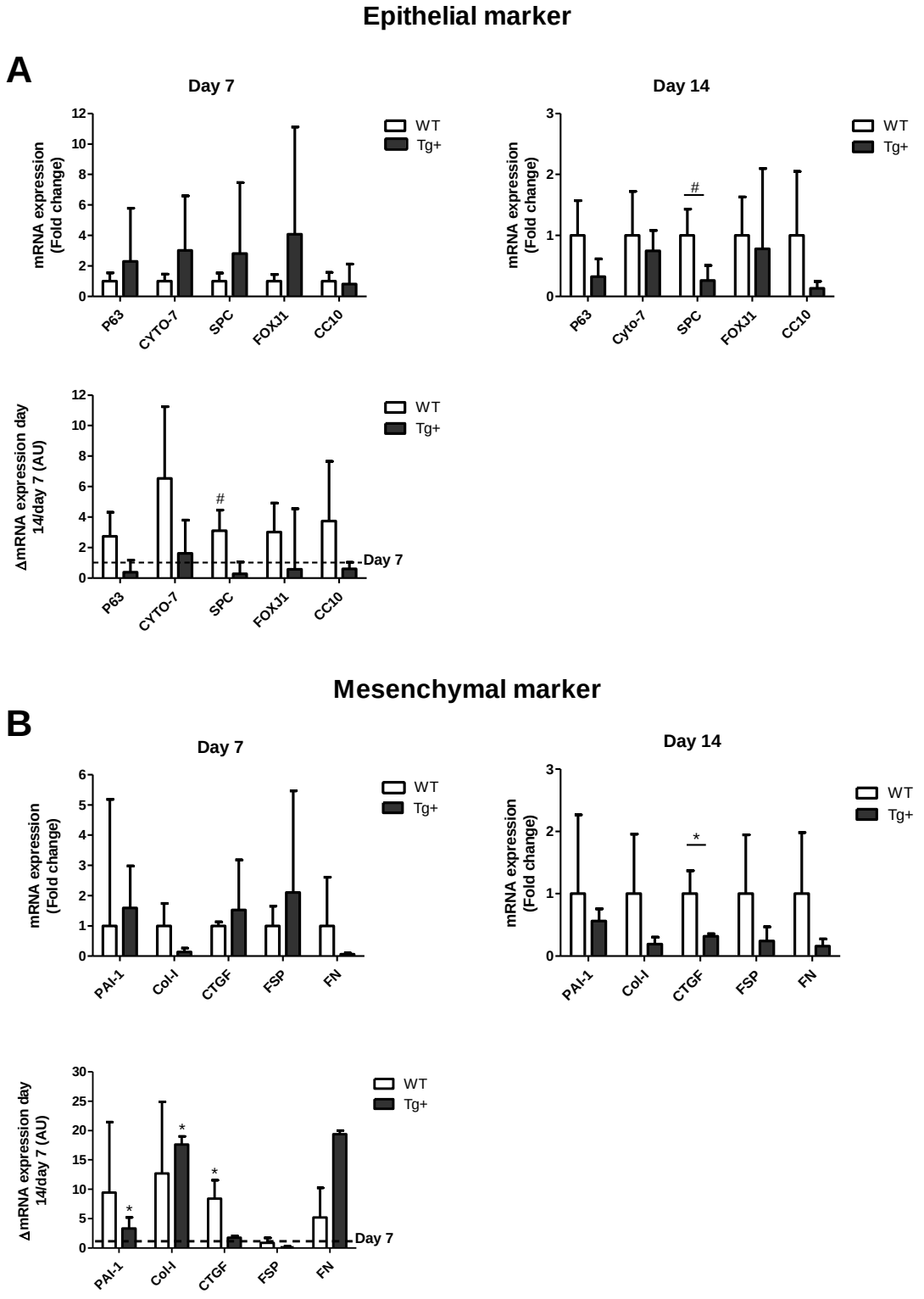

Figure 9. The diseased matrix reduces mRNA expression of epithelial and mesenchymal markers after 14 days of basal cell culture. *The expression of the epithelial markers p63, Cytokeratin-7 (Cyto-7), FOXJ1, CC10, and SPC was not significantly altered on mRNA level in basal cells that were cultured on diseased versus control matrix derived from 39-week-old SPC-TNFα mice. Only the down-regulation of SPC reaches a statistically relevant trend at day 14. However, all epithelial markers seem to become down-regulated on diseased matrix but up-regulated on WT matrix over time comparing day 7 to 14. The mesenchymal markers are also down-regulated on diseased matrix at day 14. Exceptions are seen for PAI-1, col-I, and FN which become up-regulated on diseased matrix comparing day 7 to day 14. The relative mRNA expression was measured using qPCR. Data were corrected for the expression of the housekeeping genes RPLO, YWHAZ, and RPL13A, and are expressed as mean + SD, * indicates >0.05, # indicates 0.1>p>0.05 compared to controls.*

3.5.3. ATII differentiation of MTECs was confirmed through IHC staining

The mRNA data of day 7 indicated that the SPC, the most commonly used ATII cell marker, tends to be up-regulated under diseased conditions but starts to decline upon prolonged cell culture of basal cells. To confirm that basal cells differentiate towards ATII cells, IHC staining was performed for the Tissue-specific transcription factor-1 (TTF-1) which is a specific cell protein marker for bronchiolar and alveolar epithelial cells in the lung. The results show that MTECs expressed TTF-1 on both day 7 and day 14 after recellularization in the Tg+ group. While some TTF-1 positive cells clustered at the slice border or around bronchial structures, most cells repopulated the alveolar regions under diseased conditions. In agreement with the mRNA data, the number of TTF-1 positive cells was lower at day 14 compared to day 7 in the Tg+ group. Few TTF-1 positive cells were observed in the alveolar regions of the WT group in which most TTF-1 positive cells seemed to cluster at bronchial regions.

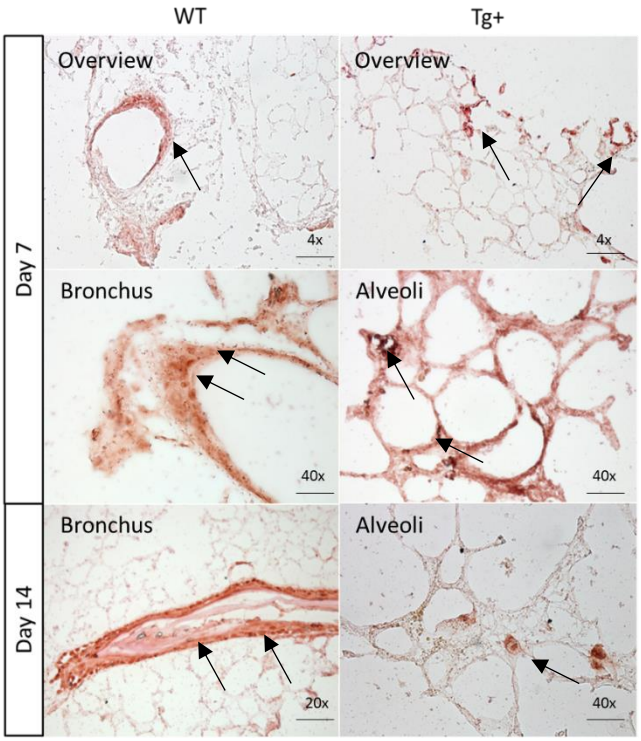

Figure 10. Immunohistochemical ATII staining in mouse lung scaffold slices under diseased and WT conditions at day 7 and 14. *TTF-1 positive cells were clustered around bronchial structures under WT conditions. In contrast, TTF-1 positive cells were present on both bronchial and alveolar regions of Tg+ scaffold slices. Images were taken at 4x, 20x, and 40x magnification. Black arrows = indicate cells.*

3.6. Immunomodulatory properties of diseased versus non-diseased matrix

COPD is characterized by chronic inflammation. Tumor necrosis factor-α (TNFα), Transforming growth factor-ß (TGFß) and Keratinocyte chemoattractant (KC) are typical pro-inflammatory molecules that are up-regulated in serum and sputum samples of COPD patients (49-51). To asses if the diseased matrix exerts immunomodulatory properties and enhances inflammatory processes in basal cells, we measured relative mRNA expression of these pro-inflammatory molecules (Figure 11 A). The molecules KC and TNFα seemed to be decreased under diseased conditions at both day 7 and day 14. However, after prolonged culture, reduction of KC reached enough statistical power to indicate a slight downward trend in the Tg+ group. TGFß did not differ between the WT and Tg+ group at any time point and instead seemed to display constant expression levels over time. When we compare mRNA expression of KC and TNFα from day 7 to day 14 (Figure 11 B), we can state that the mRNA expression tended to decrease under diseased conditions (TNFα and KC), but tended to increase under WT conditions (TNFα, TGFß, KC) with prolonged culture.

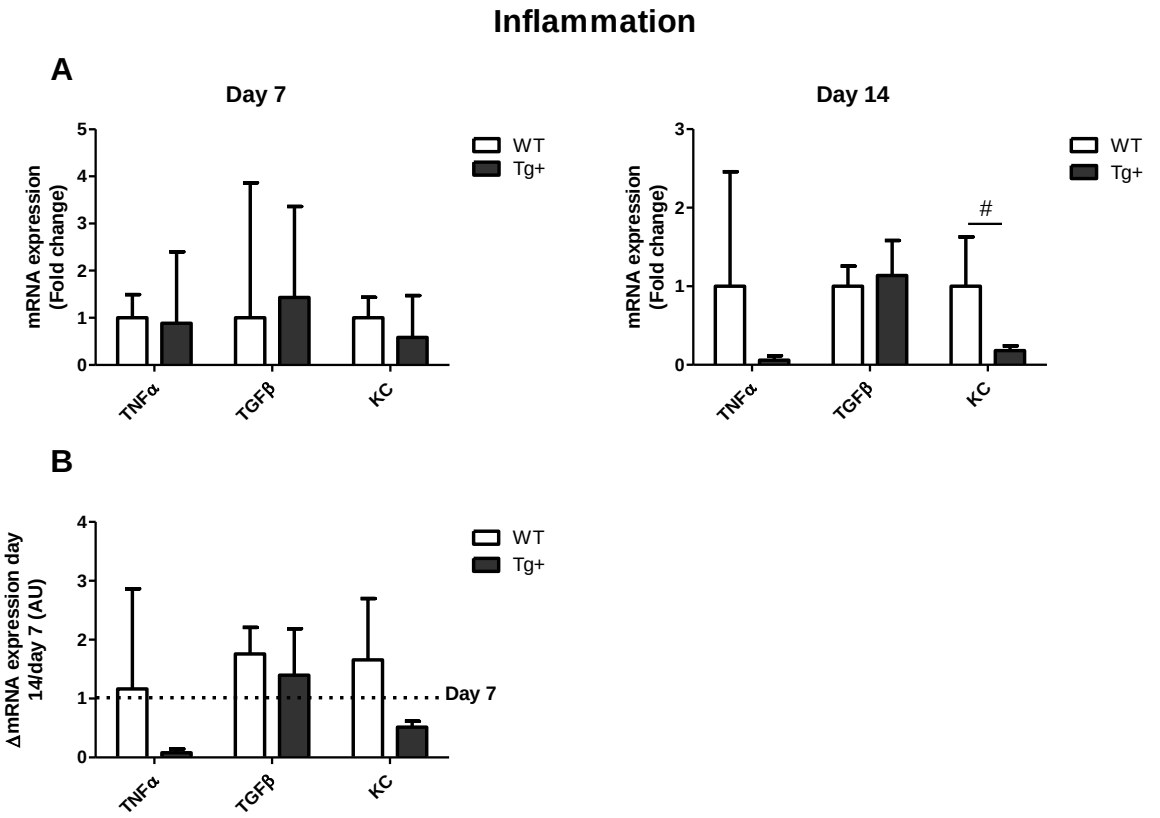

Figure 11. No significant immuno-modulatory properties are detected when basal cells are cultured on diseased matrix. *The expression of TNFα, TGFß, and KC are not significantly altered after culture of basal cells (MTECs) on diseased matrix derived from 39-week-old SPC-TNFα mice. However, KC and TNFα expression tend to decrease in cells cultured on diseased matrix over time comparing day 7 to 14. No differences are detected in TGFß expression of basal cells (MTECs) after culture on diseased versus control matrix. KC seems to be up-regulated on WT matrix at day 14. The relative mRNA expression was measured using qPCR. Data were corrected for the expression of the housekeeping genes RPLO, YWHAZ, and RPL13A, and are expressed as mean + SD, # indicates 0.1>p>0.05 compared to controls.*

3.7. Lung Hydrogel

Hydrogel derived from lung ECM provides a powerful tool to study cell-matrix interactions *in vitro*. In this study, we focused on the generation of pulmonary ECM hydrogel pooled from both SPC-TNFα mice and control littermates (Supplementary figure 7). Hydrogel is a 3D-structure and its formation results from the spontaneous self-aggregation of collagen and elastin fibres. To test if matrix proteins achieved sufficient self-assembly after isolation from decellularized tissue, hydrogels were imaged using two-photon microscopy. The results showed that the hydrogel preserves both collagen and elastin fibres in the final hydrogel solution (Figure 12). Furthermore, fibres seemed to achieve 3D-structure and did not show any signs of fragmentation. However, it should be noted that the fibres did not aggregate into clear interwoven structures as seen for intact decellularized scaffold slices, the starting material for hydrogel formation (ref. Figure 5). Besides, the intensity of the SHG signal observed for collagen was less pronounced than the intensity of the auto-fluorescent signal observed for elastin. This might indicate intrinsic differences between SHG and auto-immunofluorescent measurements. On the other hand, it might also indicate a reduced amount of collagen after hydrogel preparation which, in theory, could contribute to the convoluted nature of the hydrogel.

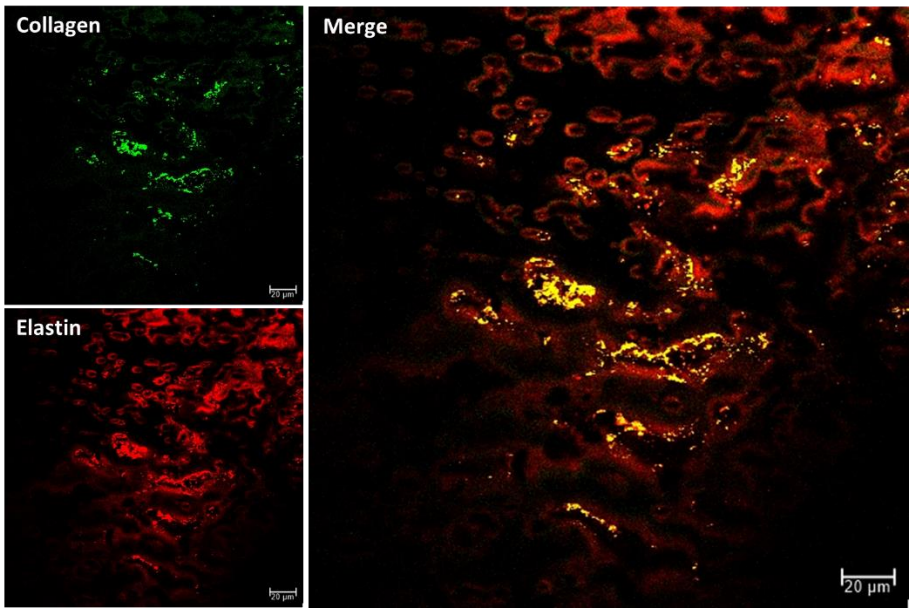

Figure 12. Collagen and elastin are present in lung ECM hydrogel. *Two-photon microscopy imaging depicted the relative abundance and distribution of collagen (green) and elastin (red) in lung ECM hydrogel. Both ECM components are preserved in the hydrogel suspension and form 3D-structures during self-aggregation. However, the interwoven network is rather convoluted in nature and differs from the clearly visible divisions of bronchi and alveoli in lung scaffold slices.*

To test whether lung hydrogel promotes cell growth and survival of basal cells, PBECs were plated and cultured upon hydrogel derived from wild-type mouse lung tissue versus a positive and negative control: a thin layer of collagen was used as positive control, whereas non-coated plastic was used as negative control. Additionally, PBECs were cultured on diseased hydrogel derived from SPC-TNFα mice to determine whether diseased matrix compromises basal cell survival and/or growth. The results illustrated that basal cells proliferated and survived on both diseased and non-diseased pulmonary hydrogel for up to 7 days in culture (Figure 13). Immunofluorescent staining for the basal cell marker P63 confirmed the presence of PBECs at day 7 in all conditions. To identify whether a diseased matrix induces stress in basal cells, stress fibres were visualized using the fluorescent-labelled protein phalloidin which specifically binds to F-actin fibres inside the cells. There were no obvious differences in stress fibre formation between (non)diseased and control conditions.

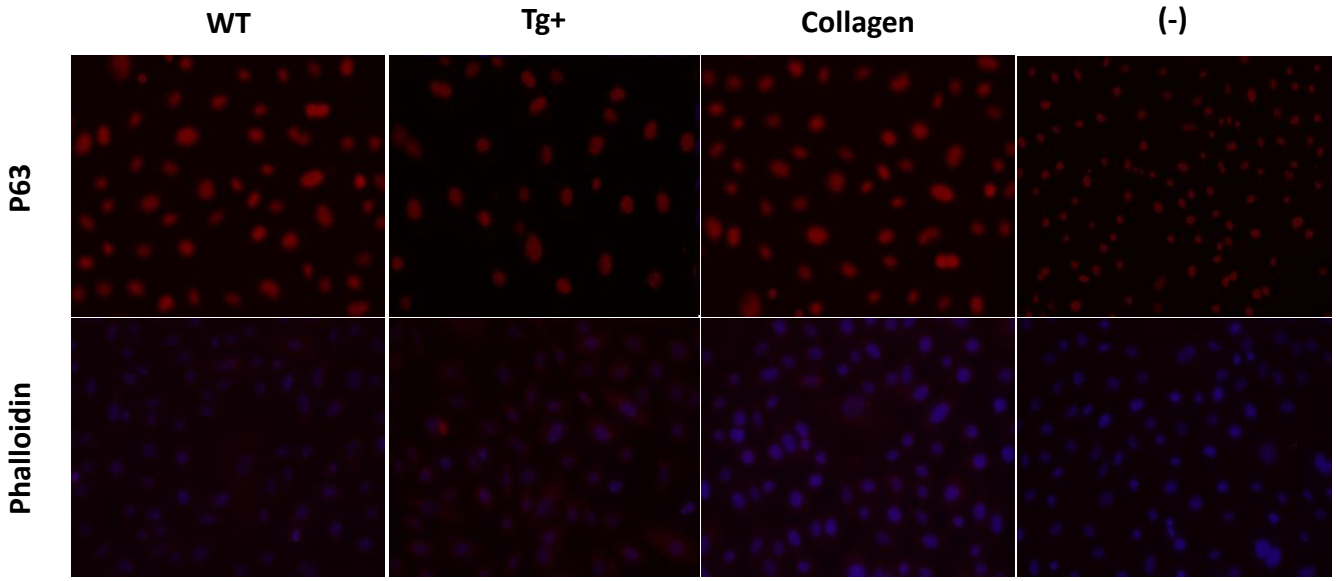

Figure 13. PBEC growth on lung ECM hydrogel. *Immunofluorescent staining of PBECs cultured on ECM hydrogel shows that the seeded PBECs are P63-positive and display no or negligible levels of stress at day 7 under all conditions (healthy (WT), diseased (Tg+), collagen (positive control), and negative control (-)). All images were taken at 40x magnitude.*

To determine whether diseased (SPC-TNFα) hydrogel impedes cell proliferation, cells were counted per relative unit surface area using imageJ. There were no significant differences between the number of cells counted on wild-type and SPC-TNFα mouse derived hydrogel after 7 days of culture (Figure 14). It seemed that both diseased and non-diseased hydrogel provided sufficient basis for cell growth and proliferation. The culture of basal cells on non-coated plastic yielded less cell proliferation per relative unit surface area compared to (non)diseased hydrogel and positive control (Figure 13). The immunofluorescent P63 staining indicated less P63-positive cells on diseased hydrogel. Therefore, it might be of interest to quantify and compare the total numbers of P63-positive cells between the

different conditions to illustrate potential differences in cell differentiation, but also to measure the ratio of P63-positive cells to DAPI-stained cell nuclei per condition.

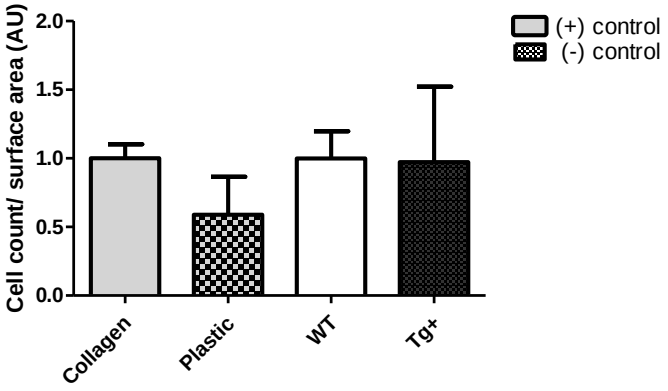

Figure 14. Relative cell count of basal cells cultured on lung hydrogel. *PBECs did grow on diseased versus non-diseased lung ECM hydrogel. The number of cells was not significantly different between positive control and hydrogel conditions at day 7. Data are expressed as mean + SD. (+) control = positive control; (-) = negative control.*

3.8. Decellularization of human lung segments and generation of human lung scaffold slices

Whole human lung samples are scarce and if they are available, they mostly originate from autopsies. Human lung segments are more readily available and are either derived from (tumor-free) biopsies or autopsies. As these segments can be small in size, segment slices would generate higher study throughput for individual study samples and further could increase their value. To date, there is limited knowledge of how to decellularize and generate lung slices from decellularized human lung scaffold segments. Therefore, we first decellularized small human lung sample pieces and generated the 300µm thick lung slices afterwards. The decellularized samples still showed signs of residual cell nuclei and smears of residual DNA (Figure 15 A). The generation of lung scaffold slices was performed by both a Krumdieck and a tissue chopper. However, the high elasticity as well as the restricted filling capacity of the individual samples resulted in convoluted slices of different size and thickness using the tissue chopper (Figure 15 B – C). No slices could be obtained using the Krumdieck. To optimize the filling capacity of the slices, the tissue segments were coated with sodium alginate and ionically cross-linked with calcium chloride. The cross-linked sodium alginate was intended to generate an artificial pleura sealing the segments and trapping the embedding medium inside the tissue. Therefore, tissue pieces were filled with LMP agarose for inflation or methylene blue for visualization. The results show that the coating was insufficient to trap the liquid inside and the fluid started to leak from the decellularized segments (Figure 15 D – E). As a result, no or little inflation of the decellularized lung segments was observed. Alternatively, decellularized lung segments were inflated using negative pressure and LMP

agarose to expel excess air and take-up embedding media instead (data not shown). However, negative pressure was not able to inflate the individual lung segments.

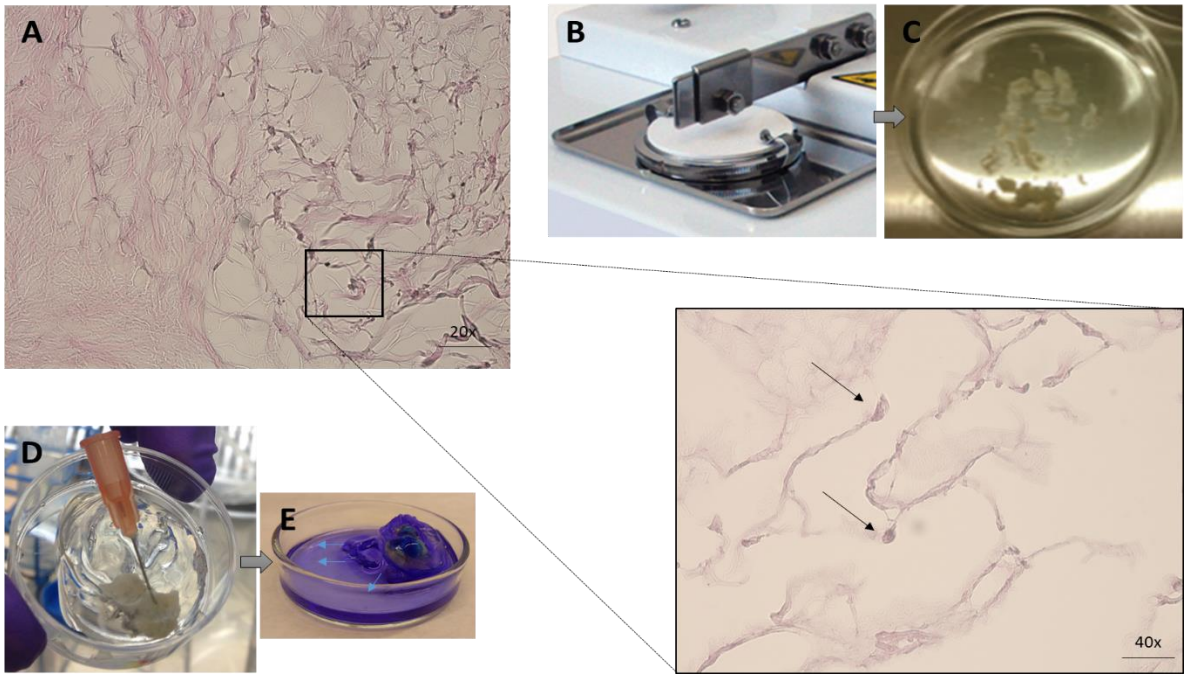

Figure 15. Decellularization, slicing, and coating of individual human lung tissue segments. *Human lung tissue samples were decellularized using incubation based decellularization and showed residual DNA smears and cell nuclei increasing the risk for immune reaction during recellularization (A). After filling with 3% LMP agarose, scaffold slices were generated using a tissue chopper (B; taken from www.tedepella.com) but were sticky, different in size, shape, and thickness (C). To optimize tissue filling, the lung segments were encapsulated using 2.5% sodium alginate and 3% calcium chloride (D). Encapsulated tissue segments were filled with either LMP agarose or methylene blue (E) using needle and syringe but did not inflate and instead appeared to be leaky.*

4. Discussion

COPD is a very heterogenous disease and arises due to many factors e.g. cigarette smoke. The disease is characterized by both chronic inflammation and emphysema. Despite its well-characterized risk profile, COPD pathogenesis remains largely unknown. There is compelling evidence that the matrix plays an important role in the induction and progression of the disease. However, until very recently it was not possible to study isolated effects of the matrix upon cell behavior as it was not possible to separate matrix and cells without rupturing ECM proteins or damaging overall ECM structure. The generation of decellularized scaffolds is novel and allows to analyse specific cell-matrix interaction(s) in an *ex vivo* model. Therefore, this study used decellularized pulmonary matrix derived from SPC-TNFα mice and littermate controls to study COPD pathogenesis and to identify pathological cell-matrix signalling in basal cells, in direct comparison with physiological conditions.

4.1. Attachment, migration, proliferation, and survival of mouse basal cells

The results indicate differences in recellularization between diseased and non-diseased lung scaffold slices. While basal cells repopulated both bronchial and alveolar regions in diseased scaffolds, they tended to cluster around the slice border or bronchial structures under wild-type conditions. The differential behavior might be associated with the induced fibrotic remodelling in the alveoli and small airways of SPC-TNFα mice: while diseased scaffolds showed enhanced deposition of collagen within alveolar regions, wild-type scaffolds contained relatively few collagen fibres in the alveoli. Under wild-type conditions, collagen was primarily found at the slice periphery or around airway structures. It is known that the mechanical properties of the ECM play an important role in the regulation of cell growth and differentiation (52). Depending on the cell type, cells can be categorized into two groups: 1) cells that are dependent on substrate stiffness and increase their proliferation with increased extracellular rigidity and 2) those that are independent of substrate stiffness and grow on both stiff and soft substrates. However, cells within the first group tend to grow poorly on soft grounds and show decreased migration under these conditions (52). Unfortunately, little is known about the substrate preferences of basal cells and whether increased stiffness in the alveolar regions might promote their initial attachment and/or proliferation. Under physiological conditions, basal cells reside in the proximal and distal airways but are absent in the more flexible and less rigid alveolar regions (53). Collagen type I and III are the most abundant types of collagen in the lung. Especially collagen type I is known to strengthen the extracellular matrix supporting the growth of epithelial cells in the airways (38). Therefore, increased extracellular stiffness could enforce initial engraftment of basal cells and

explain the enhanced outgrowth of these cells in the alveolar regions of the scaffold slice. Nonetheless, matrix rigidity and its effects on basal cell behavior need to be further elucidated.

Besides substrate stiffness and cell growth, collagen promotes and influences cell differentiation (38). Under pathological conditions, increased abundance of collagen induces EMT in alveolar epithelial cells and increases myofibroblast differentiation in COPD and pulmonary fibrosis respectively (54). Previous research at our department showed increased fractional area and increased mRNA expression of collagen type III in whole lung lysates of SPC-TNFα mice compared to wild-type littermates. Moreover, it was demonstrated that SPC-TNFα mice exhibit EMT and that TGFβ seemed to be responsible for this transition as TGFβ regulates both the expression of matrix proteins as well as protease inhibitors (1). While these changes were associated with pathological lung remodelling, they appeared to be beneficial in this study, possibly by facilitating recellularization through enhanced cell attachment and cell growth. Furthermore, it seems as though the total collagen content increases over time in recellularized scaffold slices. Although we did not quantify the increase in fractional area of collagen at day 7 and day 14 under both conditions, this could indicate that cells do not only repopulate the scaffold but are starting to deposit collagen and thereby actively remodel its matrix as was seen for stem cell spheroids (35).

Signs of active remodelling are also present upon analysis of the mRNA data in which basal cells significantly increase their collagen I expression on diseased matrix after 14 days of culture. To confirm matrix remodelling and to identify whether collagen is responsible for selective cell attachment and/or migration should be further elucidated e.g. cell tracking studies. As other matrix components such as vimentin, fibronectin, or hyaluronan are present in the ECM and play an important role in cell-matrix as well, those proteins should be assessed for relative abundance and distribution to draw further conclusions. Especially the expression of collagen IV, laminin and proteoglycan should be taken into account as those proteins reconstitute the basal membrane and should provide substrate for epithelial cell growth and attachment (55).

Another explanation for the differential attachment and growth of basal cells on diseased versus control scaffolds could be the experimental setup itself. For recellularization, decellularized tissue was sliced and plated on single wells of a 48-well plate. Cell suspensions were seeded on top of the slices and cells were incubated for at least 24 hours to allow for tissue attachment before media was replaced. The diameter of the well was specifically chosen to reduce the fractional area of uncovered plastic, mainly because pilot data indicated that in this case, cells tended to attach to the plastic instead to the tissue of interest. However, utilization of wild-type lung tissue resulted in smaller scaffold slices than those derived from diseased scaffolds due to decreased elastic properties of the emphysematous lung: the diseased lungs were less elastic, were more easily inflated with LMP agarose, and did not

recoil as fast as wild-type lungs prior to agarose hardening (56). As a result, wild-type slices did not cover the entire well and cells tended to grow on the edges and/or bottom of the well (Supplementary figure 8). The drop-wise administration of the cell suspension could have enforced the heterogenous cell distribution by pressing the cells to the edges of the well. To repopulate the entire slice, these cells would first have to attach to the edge and then slowly migrate to the centre of the slice. A possible solution would be to incubate both cells and slices under constant agitation to avoid cell cluster formation and to enhance cell-matrix contact during recellularization. Another solution would be to culture the slices on substrates that prevent cell adhesion such as non-toxic ionically cross-linked alginate (57). Besides, flow perfusion, i.e. constant movement and replacement of fluids, could be used to increase basal cell distribution across the scaffold slice *ex vivo*. In 3D cell culture, flow perfusion is preferred over static culture conditions because it is known to mimic physiological conditions and avoids the aforementioned cell cluster formation (58). Moreover, implementation of low fluid shear suspension bioreactors was shown to decrease apoptosis and to increase proliferation and total mRNA expression in ATII cells during recellularization of mouse lung scaffolds (28). In addition, fluid perfusion seems to play a role in modulating cell function: when osteoblasts were cultured with constant flow perfusion on 3D scaffolds, cells dramatically increased total matrix production and started to participate in tissue remodelling processes (59). Thus, fluid perfusion could enhance slice engraftment and cell activity during and after recellularization.

A prominent feature that was primarily observed during recellularization of wild-type scaffold slices was the formation of a diffuse layer lining the slice periphery. Although this layer was reminiscent of a keratinized membrane, it contained cells in its outermost layers and thus, could not be considered a keratinized epithelium used to protect cells and the underlying matrix from their surroundings. Furthermore, this layer did not stain positive for collagen and hence did not indicate possible collagen deposition at the apical side of the cells. However, it might be possible that the cells grew so dense that the diffuse layer resulted from the microtome slicing procedure: cutting various cells in different angles might generate a diffuse layer of cytoplasm devoid of cell nuclei. To characterize this diffuse structure and exclude other possibilities, further analysis is needed e.g. staining for cell secretion proteins.

4.2. Attachment, migration, proliferation, and survival of human basal cells

The fact that PBECs did not grow as efficiently on decellularized mouse lung tissue as MTECs can have various reasons. For instance, cell proliferation, attachment, differentiation and survival could be impeded due to species-specific differences in decellularized lungs. Although it is stated that there are no obvious substantive differences in the final decellularized lungs from different species, it is still possible that species-specific differences, e.g. the relative ratio and distribution of matrix proteins

and the variable retention of growth factors and other signaling molecules, reduce the repopulation of mouse lung scaffolds using human cells (60). As a contradiction, a human lung cancer cell line, A549, has been reported to grow efficiently on rodent decellularized lung tissue. However, there were significant differences in the experimental setup between the A549 and our study. For the human lung cancer cell line, A549 cells were continuously perfused through the lung matrix using a roller pump to ensure efficient cell distribution during recellularization. Afterwards, cells and slices were cultured using a bioreactor providing oxygenation and constant movement of fluids. In our study, PBECs were suspended in LMP agarose and perfused one-time through the cannulated trachea and consequently the entire respiratory system. The viscous pre-mixed agarose-cell suspension was intended to open the lung structure and distribute the cells using the right amount of pressure. The pressure is needed, mostly because decellularized pulmonary matrix tends to collapse in the absence of cells and surfactant (34). During cell culture, cells were not provided with constant oxygenation or flow perfusion. However, it might be possible that PBECs require constant fluid stress and oxygenation provided by a bioreactor to support cell proliferation and survival considering the direct comparison of both studies. During the respiratory cycle, epithelial cells are continuously exposed to alternating levels of mechanical and chemical stresses. While normal lung function is maintained under these conditions, changes in mechanical and chemical stresses may alter signaling pathways and therefore might have profound effects on the initial attachment and function of epithelial cells themselves (42). A lack of stretch, oxygenation, and fluid stress could therefore explain the poor repopulation of PBECs on lung scaffold slices. In alveolar epithelial cells, it was shown that mechanical forces are needed to support cell growth and differentiation (42). However, MTECs grew on scaffold slices without any need for additional stimulation.

Alternatively, it is possible that PBECs were sensitive to the slicing procedure right after lung recellularization. Slicing involves mechanical sectioning of the tissue and exposes the cells to harsh mechanical forces. Although the lungs were kept in pre-warmed PBS solution at 37°C during and after slicing, and although the slices were generated and transferred to cell culture media relatively quickly, many PBECs might not have survived this procedure.

Another possible explanation for the limited cell growth of human basal cells on mouse lung scaffolds could be the respective number of cells used for recellularization. Previous research during my junior practical internship stressed that the initial seeding density determines the efficacy of lung recellularization: if cells fail to make sufficient cell-cell contact, they fail to repopulate the entire scaffold (61). In this study, the initial seeding density was based on the relative number of cells that is typically used for mouse epithelial cell recellularization, i.e. one million cells per mouse lung (62). In comparison, the study using A549 cells for mouse lung recellularization described above, instilled fifty times as much cells per mouse lung (52). Therefore, adaptation(s) of the initial seeding density

might optimize the entire recellularization process. A starting point could be derived from common cell culture protocols in which PBECs are plated on collagen coatings at an initial seeding density of 7000 cells/cm². As 10 to 20 lung slices of each 300µm thickness can be obtained per lung scaffold, the initial seeding density of PBECs would need to be scaled up to minimally 4 to 5 million cells per mouse lung.

4.3. Epithelial barrier formation

The results of this study indicated that mRNA expression of ZO-1 is decreased under diseased conditions when compared to controls. The mRNA expression level of E-cadherin did not vary much between both conditions. In COPD patients, expression of both barrier molecules, E-cadherin and ZO-1, is decreased (56). The fact that ZO-1 is decreased on diseased matrix at both time points, day 7 and 14, could indicate a trend towards impaired barrier formation of basal cells. On the other hand, decreased ZO-1 expression could also reflect ongoing cell proliferation on the scaffold slice as ZO-1 expression is down-regulated in proliferating cells (57). To discriminate between effects of the matrix and effects of cell proliferation, it would be important to test for the expression of the proliferative marker Ki-67. Over time, mRNA expression of ZO-1 and E-cadherin tended to increase in both conditions. As these proteins are involved in cell adhesion and the formation of inter-cellular contacts, the observed time-dependent up-regulation of mRNA could also result from natural formation of cell-cell contacts during scaffold repopulation, independent of inductive effects of the underlying matrix. When cells start to repopulate the slice, they need to stabilize contacts with neighbouring cells in order to stay alive (63). Nonetheless, the results are based on mRNA expression and should be confirmed on protein level. Additionally, trans-epithelial resistance (TER) measurements are needed to test for impaired protein function and barrier formation. As those TER measurements cannot be performed on scaffold slices, they would have to be performed on basal cells grown on diseased versus control lung ECM hydrogel.

4.4. Differentiation

To assess if the diseased matrix results in adverse basal cell differentiation promoting mucus cell hyperplasia or EMT, different epithelial and mesenchymal markers were assessed at mRNA level. The results indicated an up-regulation of most epithelial and mesenchymal markers on diseased at day 7, which was followed by down-regulation of these markers matrix at day 14. This temporal shift in mRNA expression could indicate that basal cells become progressively dysfunctional when cultured on diseased matrix. In the WT group, both epithelial and mesenchymal markers increased over time indicating beneficial effects of non-diseased matrix on basal cells on transcript level. However, quantification of the total number of cells is needed to confirm these observations.

Interestingly, PAI-1 and collagen type I became up-regulated under diseased conditions comparing mRNA expression from day 7 to day 14. PAI-1 is a strong inhibitor of the plasminogen activator protein. The active form of plasminogen, plasmin, induces the degradation of various types of ECM proteins including fibronectin and proteoglycan. Under physiological conditions, PAI-1 maintains matrix homeostasis by inhibiting the breakdown of these matrix proteins (64). In chronic respiratory diseases such as idiopathic pulmonary fibrosis (IPF) and COPD, increased expression of PAI-1 seems to be associated with fibrotic lung remodelling. Moreover, patients with COPD have higher serum and sputum levels of PAI-1 (65). The fact that two (pathological) mesenchymal markers become up-regulated after prolonged culture of basal cells on diseased matrix might indicate that cells start to undergo EMT: both proteins promote collagen accumulation which in turn increases the rigidty of the matrix correlating with adverse mechanotransduction as active inducer of EMT (66). Another mesenchymal marker, is the connective tissue growth factor (CTGF). Despite initial up-regulation, CTGF was significantly decreased in the Tg+ group after 14 days of culture indicating that the diseased matrix negatively affects CTGF expression in basal cells, at least on mRNA level. In COPD, CTGF is up-regulated on both mRNA and protein level of human airway and alveolar epithelial cells and seems to be associated with EMT and increased COPD severity (67). Under physiological conditions, CTGF is expressed by various cell types and seems to be involved in cell proliferation, cell adhesion, and wound repair (68). A decrease of CTGF under diseased conditions and an increase of CTGF under wild-type conditions may indicate a lack of cell proliferation and adhesion of basal cells on diseased scaffolds and simultaneously illustrate preserved cell functionality on healthy matrix, whereby cells are capable of depositing their own matrix.

An important epithelial cell marker needed for cell repair after injury, is the Club cell marker CC10. After lung injury, Club cells start to proliferate and differentiate into different epithelial cells similarly to basal cells (69). The results indicate that CC10 expression decreases under diseased conditions. This could indicate a reduction of an important stem cell source as a result of an underlying diseased matrix. Moreover, Club cells are also known to produce and secrete the club cell secretory protein-16 (CC16), cells within the airways (70). In the context of COPD, CS induced airway CC16 deficiency increases pulmonary inflammation and injury and likely contributes to the pathogenesis of COPD (70).

The protein SPC is a marker for ATII cell differentiation in the lung. As seen for most epithelial markers, the mRNA expression of SPC was increased on day 7 but decreased at day 14 in contrast to wild-type conditions. Although not significant, these results might indicate that diseased matrix does not support long-term differentiation or sustained survival of ATII cells. As ATII cells play an important role in replacing ATI cells after injury, reduction of ATII cells would also impede alveolar regeneration (71).

To test for ATII differentiation based on protein expression data, we stained for TTF-1, a marker for bronchial and alveolar epithelial cells, using IHC staining. IF TTF-1bpositive cells are encountered around bronchi, they are considered epithelial cells, and if cells are located in alveolar regions they are considered alveolar cells. IHC staining confirmed that TTF-1 positive cells are likely to be reduced in alveolar regions with prolonged culture under diseased conditions. The increased mRNA expression of SPC in the WT group from day 7 onwards could not be confirmed with IHC staining. The fact that cells were mainly TTF-1 positive around bronchial tissue in the WT group could indicate that most cells do not differentiate towards ATII cells on non-diseased matrix. Interestingly, this could also indicate important differences between cell-matrix signaling in health and disease. In theory, the diseased matrix could trigger changes in signaling pathways of epithelial cells, for example up-regulate adverse signaling in basal cells, such as pathological Wnt signaling. Expression of Wnt5A is known to be implicated in the control of stem cell differentiation. It is upregulated in isolated cells from COPD patients which induces inflammation in the lung and inhibits alveolar expression of SPC (72). Therefore, it might be interesting to measure changes in the mRNA and protein expression of proteins important for intracellular cell signalling, especially Wnt signaling.

Other studies have performed experiments with human ATII cells as well and stated that it is difficult to keep these cells differentiated when cultured *in vitro* (73). If ATII cells are cultured *in vitro*, ATII cells tend to rapidly lose cell function including the expression of surfactant protein C and start to differentiate into ATI cells within a few days. This ATII-ATI transition could explain the observed decrease in the number of ATII cells after 14 days of cell culture. Although the maintenance of cell characteristics depends on various factors, a recent study demonstrated that 1% FBS was important to maintain biological characteristics of human ATII cells. Although we cultured basal cells *ex vivo*, it could be that the basal cells display similar properties after differentiation towards ATII cells *ex vivo* as described for *in vitro* culture. Moreover, we did not supplement the medium with 1% FBS. To test whether ATII cells differentiated towards ATI cells on scaffold slices, cells should also be tested for the expression of alveolar type I marker such as aquaporin 5 (74).

Furthermore, as suggested above, changes in mechanical stresses may also affect ATII differentiation (42). While it is known that deep inspiration stimulates surfactant release in vivo, it has been demonstrated that repeated or single stretch applied to cultures of primary rat ATII cells causes an increase in intracellular surfactant secretion as measured by phosphatidylcholine release (42). In conclusion, it would be interesting to test if ATII differentiation increases after stretch of decellularized slices. However, this would also make it difficult to delineate individual effects of the matrix and stretch respectively.

Lastly, it should be mentioned that cell expression may change in the presence of other cell types. In this study, basal cells were cultivated isolated from other cell types of the lung that might impact expression and functionality of basal cells as well.

4.5. Immunomodulatory properties

The diseased matrix seems to exert little immunogenic properties on basal cells. Neither TGFß, TNFα, nor KC expression were significantly altered on mRNA level. Although not significant, the keratinocyte chemokine, KC, seems to be decreased under diseased conditions, while it seemed to increase under wild-type conditions at both time points. These results did not match our expectations, as KC is a strong chemoattractant for neutrophils. In COPD, increased expression of KC correlates with increased inflammation and disease severity. Therefore, we expected the cells to display increased levels of KC under diseased conditions (51). The pro-inflammatory cytokine TNFα shows similar results regarding its mRNA expression. Although TGFß is known to be a potent inducer of CTGF and PAI-1 expression, the mRNA expression of TGFß did neither vary between the different conditions nor did it vary in time. It should be noted that all observations were based on relative mRNA expression. Therefore, these results do not reflect possible changes and/or post-translational modifications on protein level. To exclude immunomodulatory properties within the diseased matrix, other inflammatory molecules should be assessed as well and should be confirmed by western blot or IHC/IF.

4.6. Lung hydrogel

As part of this study, we wanted to validate pulmonary hydrogel as tool to study cell-matrix interactions in health and disease, mainly because hydrogel recapitulates the structure and composition of ECM *in vitro.* Therefore, it is more physiologically relevant than the commonly used cell substrate coating using single matrix components. Matrigel is a commonly available natural cell culture substrate which contains various ECM proteins such as collagen and laminin as well as growth factors such as TGFß or PDGF (38) to mimic ECM properties *in vitro.* In comparison with Matrigel, pulmonary hydrogel is expected to preserve more lung specific proteins including small molecules and growth factors, which is more suited for lung tissue-specific cell culture. In addition, pulmonary hydrogel is expected to maintain disease characteristics such as decreases in elastin and increases in collagen content. In our preliminary experiments, we were not able to identify significant differences between cells grown on diseased versus cells grown on control hydrogel with regards to proliferation and P63 expression. A more thorough investigation into cellular behaviour on controls versus diseased hydrogel is necessary. It should also be examined whether the relatively harsh procedure for the generation of lung hydrogel diminishes disease characteristics and could disrupt important properties of the original scaffold: as collagen and elastin fibres need to re-assemble spontaneously, they might not re-develop

fibrotic or emphysematous matrix characteristics. To this end, the structure and composition of hydrogel derived from control versus diseased lung tissue should be studied performing i.e. western blotting, mass spectrometry, 2-photon and scanning electron microscopy. A diminishment of disease characteristics as consequence of the method itself could explain the lack of difference(s) observed in cell growth between diseased and control hydrogel. Besides, not all cells might have stained P63-positive. There might be differences in cell differentiation between the different conditions and should be evaluated as well e.g. the ratio between P63-positive cells and DAPI-stained cells per condition.

Nonetheless, this study validates the implementation of hydrogel as tool to study cell behavior on naturally derived ECM *in vitro*. The results show that basal epithelial cells maintain P63 expression and do not undergo obvious apoptosis. Moreover, cell culture using hydrogel coating resulted in equal number of cells per relative surface area in comparison with cell growth on collagen coating, the positive control, which highlights the beneficial properties and bioactivity of the generated hydrogel. In follow-up experiments, cells should be cultured until confluency to examine their capability to establish functional cell-cell contacts and adhesions, e.g. by using immunofluorescent staining for E-cadherin and ZO-1. In addition, cell should be cultured at ALI to assess barrier function (TER measurements) and cell differentiation (number of ciliated cells) on hydrogel.

4.7. Decellularized human lung scaffold slices

Decellularized human lung tissue was used to generate human lung scaffold slices. The decellularization process was relatively efficient and yet should be further optimized. Histological assessment of individual scaffold slices showed residual nuclei and smears of residual DNA. Although small in number, these remaining cells could be immunogenic and therefore detrimental for cell culture experiments. The problem of decellularizing tissue pieces is that the detergents need more time to penetrate the entire tissue, as instillation of detergents using mechanical forces (e.g. pressure) is only possible if an intact airway or vasculature is present. Therefore, it might be of interest to optimize the volume and concentrations of the decellularization detergents and/or the time of incubation corresponding to the size of the tissue piece. In addition, it might be worth considering to first slice the tissue, and then decellularize it in order to reduce the time and relative amount of detergents needed for the entire process. Another alternative would be to stretch the tissue, as seen for toxicologic studies, to enhance the penetration of the detergents during incubation (75).

Apart from efficient decellularization, cell culture studies need clear and reproducable experimental conditions. Any differences in slice thickness could interfere with the results and should be avoided (76). However, the generation of equal human lung scaffold slices faced many obstacles. First, decellularized human tissue pieces were too soft to slice. Human tissue pieces are mostly obtained

from distal regions of the lung after e.g. lung resection and therefore, these tissues do not contain intact vasculature or airway structures, which are needed to instil embedding media such as LMP agarose to harden the tissue prior to slicing. Without instillation, the embedding medium fails to penetrate and stiffen the entire tissue. In our experimental set-up, we tried to incubate the tissue with 3 to 10% LMP agarose as long as possible, so that the pieces had enough time to soak up the embedding medium before we let them harden in PBS solution at 4°C or leaving them *en bloc* in agarose. However, the major problem was that the tissue pieces retained too much air. Instillation of detergents is able to replace the air with detergent solution, while incubation with detergents does not. To circumvent this obstacle, we tried to apply negative pressure expelling the air and replacing it with LMP agarose. Nonetheless, the decellularized tissue pieces were not elastic enough to stretch and soak up the agarose. A reason for this might be the fact that decellularization is associated with loss of elastin rendering the tissue less elastic (48). A possible solution could be to stretch the tissue using a clip on each side of the tissue to stretch it vertically in an organ bath or using a stretch bioreactor to promote release of excess air and drive the uptake of embedding medium (77).

Another strategy was to seal the decellularized lung tissue pieces with non-toxic ionically cross-linked sodium alginate. Excised lung segments lose pulmonary pleura and are therefore not able to retain any solutions e.g. solubilized embedding media. Other studies reported that the implementation of alginate as an artificial pleura would permit inflation of small acellular lung segments, and significantly enhances retention of cells inoculated through cannulated airways or blood vessel (57). We sealed the decellularized human lung tissue pieces using sodium alginate, cross-linked with calcium chloride, and instilled the media using a syringe. However, the tissue piece did not inflate indicating that the seal did not cover the entire tissue, became leaky or that the viscosity of the embedding media was too high and generated pores into the alginate coating. In addition, it might be possible that intact vasculature or airway structures are needed to distribute the fluid, as described above. It might also be possible that excess air trapped inside the segment prevented the uptake of LMP agarose and increased the pressure inside the sealed segment creating pores. Follow-up experiments could consist of alternating the percentage of LMP agarose or using other non-toxic embedding media which hardens the tissue without binding the cells themselves. Another possibility could be to harden the tissue with a hydro-soluble embedding media such as TissueTek used for cryotome sections (78). In this experimental set-up, decellularized tissue could be embedded using the toxic chemical TissueTek and get sectioned. Prior to recellularization, the toxic chemical could be washed out using water (78).

5. Conclusion

We hypothesized that alterations of the extracellular matrix render the matrix diseased and result in adverse behavior of basal cells, which in turn diminishes epithelial integrity and drives mucus cell hyperplasia. In this context, we were able to demonstrate that the diseased matrix is able to affect the expression of epithelial and mesenchymal markers in bronchial epithelial basal cells on mRNA level. As these markers seemed to become progressively down-regulated on diseased matrix over time, this could indicate that the matrix renders basal cell dysfunctional, contributing to pathological processes observed in COPD. However, we could not identify direct proof for mucus cell hyperplasia. Epithelial integrity was not significantly affected but displayed limited expression of the barrier molecule protein ZO-1 on diseased matrix. However, further research is needed to expand and confirm these results on protein level. A major problem was to achieve full repopulation of both wild-type and diseased scaffolds, especially regarding recellularization with human basal cells. Therefore, further optimization of the methods is needed including cell seeding and the generation and cultivation of slices. Lastly, lung ECM hydrogel could be generated from both diseased and non-diseased mouse lungs and sustained basal cell survival.

6. Acknowledgements

First had foremost, I would like to thank my supervisor, **Niki**, for the opportunity to perform an internship at the Department of Respiratory Medicine. I am very thankful for all the support and trust you gave me during my internship. You were always there if I had any questions, you would always bring in ideas if I was confronted with a problem and you would always turn every obstacle into a solution, even if RNA went missing or HE staining started to fade. I would not be where I am right now, if it wasn't for you. Moreover, I would like to thank you for the support you gave me during the writing of my thesis. Although it was quite a battle in time, you would leave your door open, stay patient and assist me until the very last minute (I would like to give my excuses for all the stress I gave you on the last few days to the finish … correcting 36 pages with lots of points to adapt is not an easy job!).

Cheryl and Caspar, I want to thank you for the time I spent with you in the first two month. You were always there to assist me, introduced me to the lab and helped me wherever you could. Even though you preceded work in Vermont, you would always have an open ear, ask me how I was doing, and helped me if I encountered any problems… even if it was just to ask if there would be any chance that we (perhaps) have a DNase, an inhibitor, or some media flying around in one of the thousand fridges. I missed you both here and I hope you have a great time in America.

Mieke, thank you for your kind support and suggestions whenever I needed It, even if It was close to 5 pm or involved some urgent SOS labhelp mails. I also want to thank you for everything that was supplied by the PLUC facility to carry out this work.

I also want to thank **Marco, Chiel and Wessel** for all the support they gave me during my internship and especially in the lab. Marco, you would always have an open ear and I know I terrorized you with tons of questions every day, but I hope you know that I meant it well. During the time I spent here, I really did learn a lot of technical details from you and I will keep all the kind remarks in mind for the future. Furthermore, I hope you don't have to order any 48 well plates anymore in your life…it may take centuries. And I hope that you will manage to find the house that finally fits you. Chiel, you are a mastermind! Thank you for all your creative ideas, patience and help whenever I tended to do something wrong. I also want to thank you for the tons of wonderful DVD's that I could luckily spread to all my friends. However, I kept two… just in case. Wessel, Olá! ¿cómo estás? You did help me a lot and I just want to let you know that I am really thankful for everything you did for me and for all the tips you gave me. I know I could be very chaotic but every chaos has its logic. Moreover, I really

think that you have a lovely singing voice and you should always keep continuing dancing and singing in the lab… definitely got some spark there, plus never forget the german word I taught you.

Nico, I want to thank you for all your help! You would always listen and help me out wherever you could. More than once you did save the day!

Lynette, I want to thank you for being a great roommate! I definitely missed you and I think you will do great in Italy. Moreover, I hope we will see each other again. It was so much fun having another master student around! And I am still digesting our Master cake… but it was definitely worth it.

Sara, you are great and a very kind person. Besides, you are a very good and crazy lab partner. Your Nescafe did bring me through the last stages of writing, no doubt! I also fell in love with your little son, he really will become a womanizer one day. And I will visit and make you some tasty food as well!

Martijn, thank you for tagging me in nearly almost every meme that had the words deadline or thesis in it! I don't know how you did it, but it definitely kept me going.

Darcy, I would like to thank you because of all the things you taught me… I could use so much of it now, writing this thesis. You would even help me out although you faced some new challenges yourself. I am so glad to have had that time in Munich with you!

Lastly, I want to thank everyone that was part of my journey here in Maastricht: **Stephanie, Karin, Juliette, Rosanne, Mieke, Jules, Pieter, Anita, Harry, Ramon, Coby, Wouter, Sarah, Desiree, and Clarie.**

7. Supplementary

7.1. Supplementary protocols

7.1.1. Immunofluorescent PBEC characterization

A subset of PBECs used for recellularization was cultured on Labtek chambers (Thermofisher, The Netherlands) until they reached 80-90% confluency. Labtek chambers were washed 3x with 1xPBS after removal of culture media. The cells were fixated using 4% PFA for 30 minutes at RT. Next, slices were washed 3x with 1xPBS. Then, cells were permeabilized and blocked using 0.1% Triton X-100 in 1% BSA/PBS for 20 minutes. Afterwards, cells were washed 3x with 1xPBS. The primary antibodies mouse monoclonal anti-P63 antibody (1:1000; Santacruz, USA), rabbit anti-Cytokeratin 5/6 (1:1000; Covanco, USA), and mouse anti-MNF116 (1:200; Abcam, The Netherlands) were diluted in 1% BSA/PBS and incubated over night at 4°C. After 3x wash with 1xPBS, the cells were incubated with the secondary antibodies, 1000x diluted in 1% BSA, goat anti-mouse Alexa555 and goat anti-rabbit Alexa555 (Dako, the Netherlands) respectively and kept for 20 minutes in the dark at RT. Next, cells were washed 3x in 1xPBS and nuclei were counterstained using 2.5µl of 200 µg/ml DAPI (Sigma-Aldrich, Germany) per 1ml 1xPBS for 5 minutes in the dark at RT. Then, cells were washed 2x with 1xPBS and 1x with ddH20. Sections were mounted using Faramount (Dako, the Netherlands), dried for 30 minutes at 37°C, and stored at 4°C until ready for imaging. Negative controls were made using no primary but only secondary antibodies by incubating the samples with 1% BSA/PBS over night at 4°C.

7.1.2. Real time PCR (qPCR)

All cDNA samples were thawed and 25x diluted using nuclease (DNase/RNase free) H2O (Thermofisher Scientific, The Netherlands). For each target, a qPCR mastermix was prepared consisting of nuclease free H2O, SyBr green mix, 10 pmol/µl forward and reverse primer solution (Supplementary table 1). The qPCR mastermix was gently mixed and centrifugated at 3000 RPM. Next, ¼ cDNA is added to ¾ of the qPCR mastermix in a 384 well plate. After a short spin at 1200 RPM, qPCR was performed using the LightCycler 480 (Roche, Germany) and a melting temperature (Tm) of 55°C. The specificity of the amplification was verified by melt curve analysis and evaluation of efficiency of PCR amplification. Primers were designed to anneal at 60 to 65°C and to generate a PCR amplification product of 100 to 150 bp. Transcript levels for the constitutive housekeeping gene products cyclophilin A, RPL13A, and YWHAZ were quantitatively measured in each sample to control for sample-to-sample differences in RNA concentration.

7.2. Supplementary tables

Table 1. List of primer sequences.

Gene	Forward primer	Reverse primer
P63	AACGGCTCCTCGTCCACCAG	GCAGGGGATGGAGAGAGGGC
Cyto-7	GCTGCTGGAGGGCGAGGAG	CACCATTGCCCCCAGTGGA
pro-SPC	AGACTCTGGCTGTGGAGGAG	GGTGACGGTGTTGTCCTCAT
FOXJ1	GCATCGACCCCCAGTACGCA	GCGCTAGGTTCCTGGGAGGC
CC10	AGGCCCTCCTCATGGAATCAGAGT	TCAGCTGGGTGCCCGCATTT
PAI-1	AGT CTT TCC GAC CAA GAG CA	GAC AAA GGC TGT GTG GAG GAA G
Col-I	TCGGAACTGCAGAGACCTAAA	CCCCAGTTTCCATGTTACAGA
FN	GTG TAG CAC AAC TTC CAA TTA CGA A	GGA ATT TCC GCC TCG AGT CT
CTGF	CACAGAGTGGAGCGCCTGTTC	GATGCACTTTTTGCCCTTCTTAATG
FSP	CTG GGG AAA AGG ACA GAT GA	TGC AGG ACA GGA AGA CAC AG
TGFß	TGGGACCCTGCCCCTATATTTG	CGCCCGGGTTGTGTTGG
ZO-1	GTCCTGAAGCCCGTGGAGCTAC	TAATTCGGATCTCCAGGAAGACACTT
E-cad	CCCCAGTATCGTCCCCGTCC	GGTCGCTGTCGGCTGCCTT
TNFα	CAGCGCTGAGGTCAATCTGCC	TGCCCGGACTCCGCAA
KC	CAA AAG ATG CTA AAA GGT GTC CCC A	CGT TCA CCA GAC AGG TGC CAT
YWHAZ	TGCTGGTGATGACAAGAAAGGAA	AACACAGAGAAGTTGAGGGCCA
Cyclo	TTCCTCCTTTCACAGAATTATTCCA	CCGCCAGTGCCATTATGG
RPL13A	CACTCTGGAGGAGAAACGGAAGG	GCAGGCATGAGGCAAACAGTC

7.3. Supplementary figures

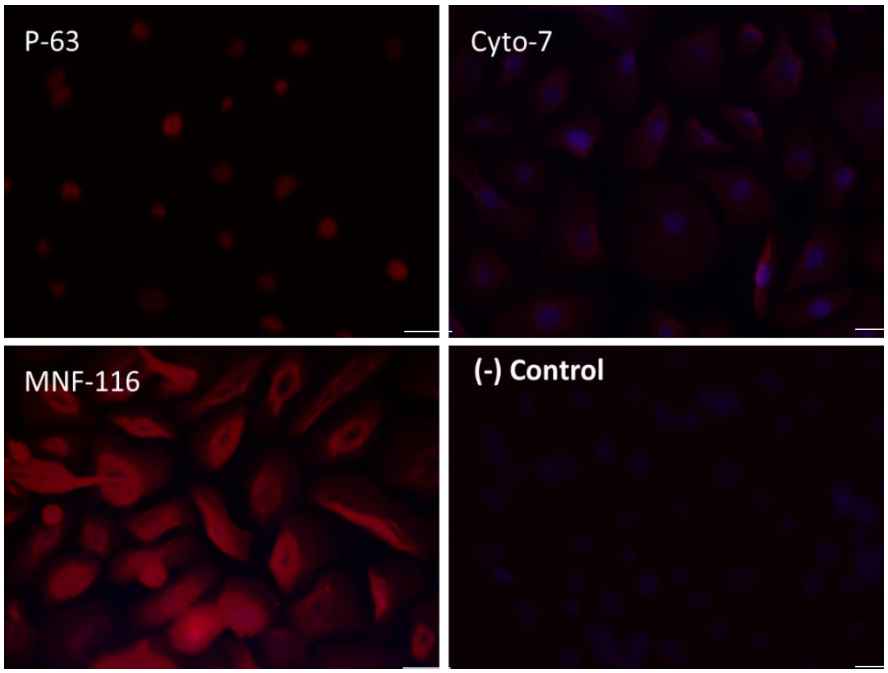

Supplementary figure 1. Immunofluorescent PBEC characterization. *The basal cells used for recellularization were characterized beforehand. Therefore, basal cells were cultured on Labtek chambers and stained for basal cell specific markers: transformation related protein 63 (P-63), Cytokeratin-7 (Cyto-7), and MNF116. All images were taken at 40x magnitude.*

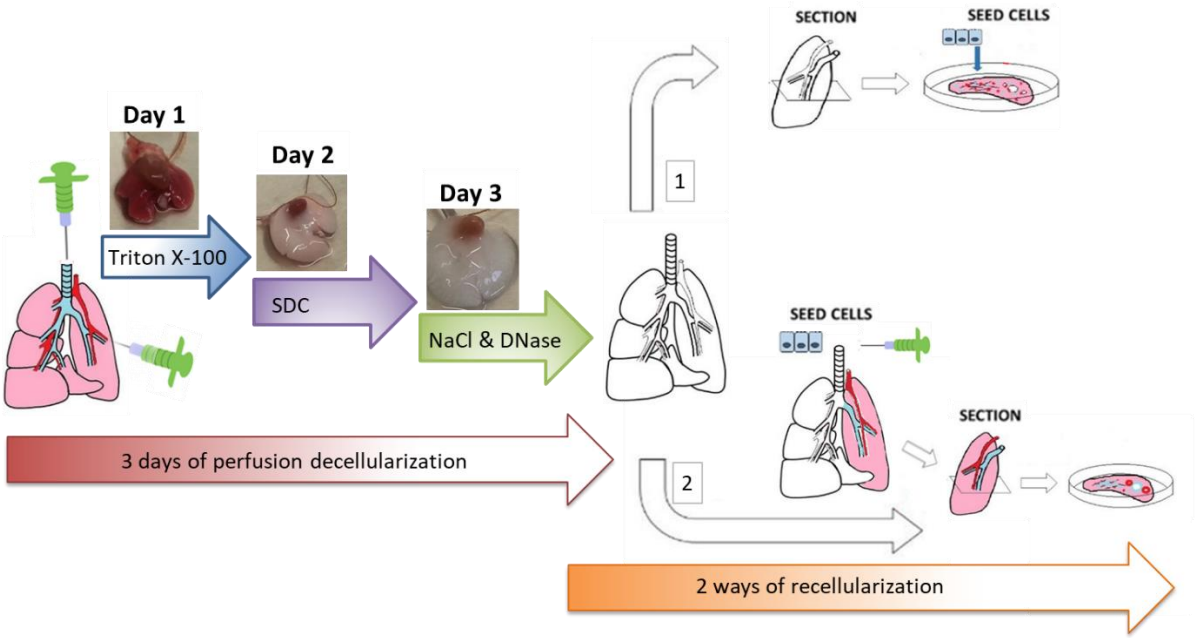

Supplementary figure 2. Decellularization and recellularization of mouse lungs. *Mouse lungs were decellularized using perfusion based decellularization whereby different detergents (Triton X-100, sodium deoxycholate (SDC), sodium chloride (NaCl), and DNase) are instilled through both airways (trachea) and vasculature (right ventricle) to induce cell lysis and degradation of intracellular proteins and DNA. The decellularized lungs consist of purified pulmonary extracellular matrix maintaining native tissue structure and composition. Therefore, they can be used as cell culture substrate to study cell-matrix interaction ex vivo. There exist two different ways of recellularization: 1) generate decellularized lung scaffold slices and seed cells on top, 2) seed slices via the respiratory system and generate slices afterwards.*

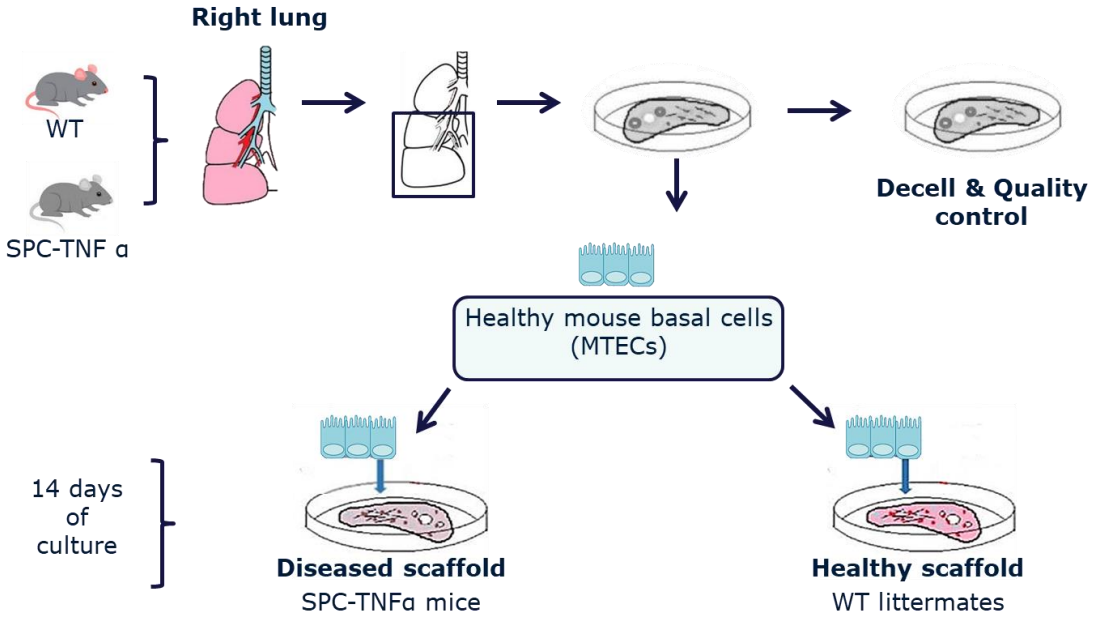

Supplementary figure 3. Mouse lung recellularization with mouse basal cells (MTECs). *Mouse lungs were isolated from SPC-TNFα and wild-type (WT) littermate mice for decellularization. Decellularized scaffold slices were generated from the right lung and a) used as decellularization (decell) and quality control including assessment of residual cell nuclei and DNA, and b) recellularization with MTECs (way 1, Supplementary figure 2).*

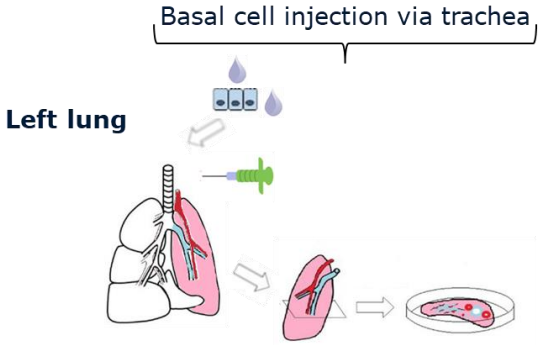

Supplementary figure 4. Mouse lung recellularization with human basal cells (PBECs). *Mouse lungs were isolated from SPC-TNFα and wild-type (WT) littermate mice for decellularization. Decellularized scaffold slices were generated from the left lung and recellularized with PBECs (way 2, Supplementary figure 2).*

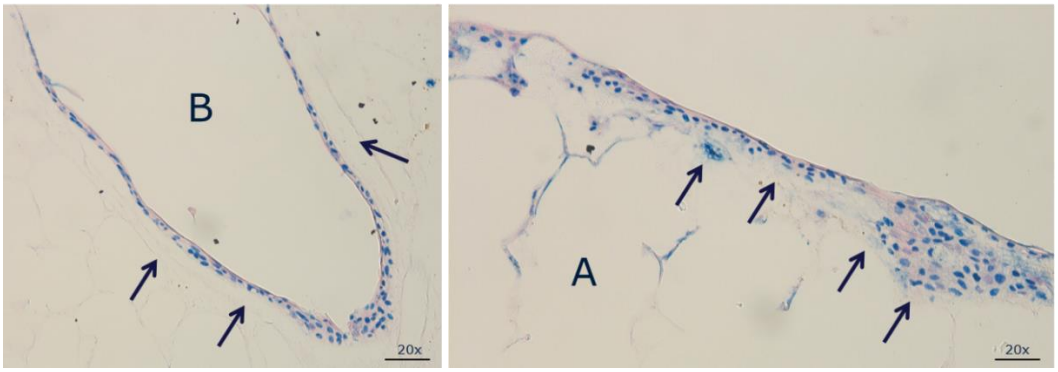

Supplementary figure 5. Mouse basal cells (MTECs) cultured on decellularized mouse lung scaffold slices were P63 positive. *300µm thick lung scaffold slices were recellularized with MTECs and immune-histochemistically stained for P63, a nuclear basal cell marker. At day 14, basal cells were primary localized at a) bronchi and b) the slice border under both diseased and non-diseased conditions. Few basal cells were localized at the slice centre. Black arrows = indicate basal cells; B = bronchus; A = alveoli.*

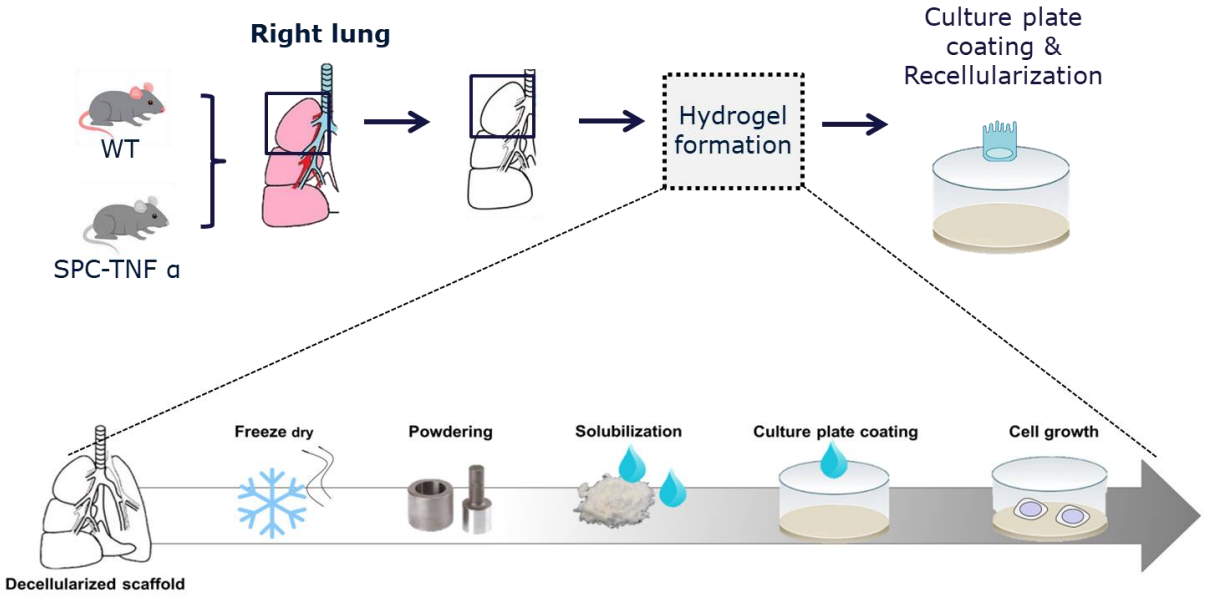

Supplementary figure 7. Generation of lung extracellular matrix (ECM) hydrogel and recellularization with human basal cells (PBECs). *The upper left lobes of decellularized SPC-TNFα and decellularized wild-type (WT) littermate mice lungs were used for hydrogel formation, whereby decellularized pulmonary scaffolds were freeze-dried to remove excess liquid and avoid crystallization, grinded to increase surface area and facilitate solubilisation of individual matrix fibres, and solubilized to coat cell culture dishes or well plates. Hydrogel formation occurs due to spontaneous aggregation of separated elastin and collagen fibres at 37°C. Afterwards, PBECs were cultured on pulmonary ECM for 7 days and assessed for P63 positivity, cell survival, and cell stress.*

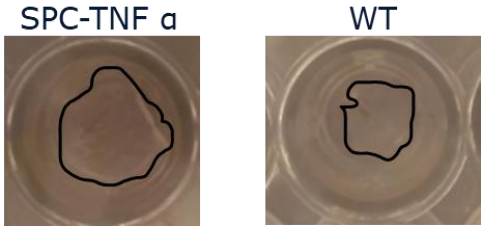

Supplementary figure 8.Decellularized SPC-TNFα and wild-type (WT) lung scaffold slices in a 48-well plate. *Decellularized SPC-TNFα lung scaffold slices are larger than WT lung scaffold slices due to due to e.g. the decreased elasticity and intrinsic recoil of diseased (emphysematous) mouse lungs. Well diameter = 11 mm; well growth area: 0.95 cm².*

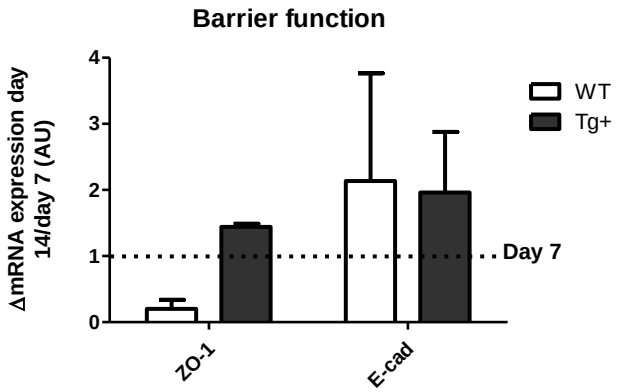

Supplementary figure 9. The diseased extracellular matrix might influence the mRNA expression level of junctional proteins over time. *The mRNA expression of ZO-1 and E-cadherin (E-cad) tend to increase over time in MTECs cultured on diseased versus control matrix derived from 39-week-old SPC-TNFα mice. Data were corrected for the expression of the housekeeping genes RPLO, YWHAZ, and RPL13A, and are expressed as mean + SD.*

8. References

1. Eurlings IMJ. Matrix remodelling in COPD, contribution of epithelial plasticity. Maastricht Maastricht University; 2015.
2. Suki B, Sato S, Parameswaran H, Szabari MV, Takahashi A, Bartolák-Suki E. Emphysema and Mechanical Stress-Induced Lung Remodelling. Physiology (Bethesda). 28. Bethesda, MD2013. p. 404-13.
3. Talag AA. Clinical physiology of chronic obstructive pulmonary disease. BCMJ, BC Medical Journal. 2008;50, No.2:5.
4. Committee GE. Global Strategy for the Diagnosis, Management, and Prevention of Chronic Obstructive Pulmonary Disease. Portland, Oregon, USA: World Health Organization; 2006.
5. Lane CR, Tonelli AR. Lung transplantation in chronic obstructive pulmonary disease: patient selection and special considerations. Int J Chron Obstruct Pulmon Dis. 102015. p. 2137-46.
6. Van Eeden SF, Sin DD. Oxidative stress in chronic obstructive pulmonary disease: A lung and systemic process. Can Respir J. 202013. p. 27-9.
7. Eurlings IMJ. Matrix remodelling in COPD; contribution of epithelial plasticity [Dissertation]: University of Maastricht; 2015.
8. Angelis N, Porpodis K, Zarogoulidis P, Spyratos D, Kioumis I, Papaiwannou A, et al. Airway inflammation in chronic obstructive pulmonary disease. J Thorac Dis. 62014. p. S167-72.
9. Crystal RG. Airway basal cells. The "smoking gun" of chronic obstructive pulmonary disease. Am J Respir Crit Care Med. 2014;190(12):1355-62.
10. Balestrini JL, Niklason LE. Extracellular matrix as a driver for lung regeneration. Ann Biomed Eng. 2015;43(3):568-76.
11. Iwasaki A, Foxman EF, Molony RD. Early local immune defences in the respiratory tract. Nat Rev Immunol. 2017;17(1):7-20.
12. Annoni R, Lancas T, Yukimatsu Tanigawa R, de Medeiros Matsushita M, de Morais Fernezlian S, Bruno A, et al. Extracellular matrix composition in COPD. Eur Respir J. 2012;40(6):1362-73.
13. Dentener MA, Vernooy JH, Hendriks S, Wouters EF. Enhanced levels of hyaluronan in lungs of patients with COPD: relationship with lung function and local inflammation. Thorax. 2005;60(2):114-9.
14. Burgess JK, Mauad T, Tjin G, Karlsson JC, Westergren-Thorsson G. The extracellular matrix - the under-recognized element in lung disease? J Pathol. 2016;240(4):397-409.
15. Rock JR, Randell SH, Hogan BL. Airway basal stem cells: a perspective on their roles in epithelial homeostasis and remodelling. Dis Model Mech. 2010;3(9-10):545-56.
16. Rock JR, Onaitis MW, Rawlins EL, Lu Y, Clark CP, Xue Y, et al. Basal cells as stem cells of the mouse trachea and human airway epithelium. Proc Natl Acad Sci U S A. 2009;106(31):12771-5.
17. Hong KU, Reynolds SD, Watkins S, Fuchs E, Stripp BR. In vivo differentiation potential of tracheal basal cells: evidence for multipotent and unipotent subpopulations. Am J Physiol Lung Cell Mol Physiol. 2004;286(4):L643-9.
18. Zheng D, Soh BS, Yin L, Hu G, Chen Q, Choi H, et al. Differentiation of Club Cells to Alveolar Epithelial Cells In Vitro. Sci Rep. 2017;7:41661.
19. Mao P, Wu S, Li J, Fu W, He W, Liu X, et al. Human alveolar epithelial type II cells in primary culture. Physiol Rep. 2015;3(2).
20. Randell SH. Airway Epithelial Stem Cells and the Pathophysiology of Chronic Obstructive Pulmonary Disease. Proc Am Thorac Soc. 32006. p. 718-25.
21. Randell SH. Airway Epithelial Stem Cells and the Pathophysiology of Chronic Obstructive Pulmonary Disease. Proceedings of the American Thoracic Society. 2006;3(8):718-25.

22. Schamberger AC, Staab-Weijnitz CA, Mise-Racek N, Eickelberg O. Cigarette smoke alters primary human bronchial epithelial cell differentiation at the air-liquid interface. Sci Rep. 2015;5.
23. Zuo WL, Yang J, Gomi K, Chao IW, Crystal RG, Shaykhiev R. EGF-Amphiregulin Interplay in Airway Stem/Progenitor Cells Links the Pathogenesis of Smoking-Induced Lesions in the Human Airway Epithelium. Stem Cells. 2017;35(3):824-37.
24. Wittekindt OH. Tight junctions in pulmonary epithelia during lung inflammation. Pflugers Arch. 469. Berlin/Heidelberg2017. p. 135-47.
25. Schlingmann B, Molina SA, Koval M. Claudins: gatekeepers of lung epithelial function. Semin Cell Dev Biol. 2015;42:47-57.
26. Crystal RG. Airway Basal Cells. The "Smoking Gun" of Chronic Obstructive Pulmonary Disease. Am J Respir Crit Care Med. 2014;190(12):1355-62.
27. Scitable by Nature Education ACPfSS. Essentials of Cell Biology, Cell signalling: Nature Education; 2017.
28. Crabbe A, Liu Y, Sarker SF, Bonenfant NR, Barrila J, Borg ZD, et al. Recellularization of decellularized lung scaffolds is enhanced by dynamic suspension culture. PLoS One. 2015;10(5):e0126846.
29. Lele TP, Sero JE, Matthews BD, Kumar S, Xia S, Montoya-Zavala M, et al. Tools to study cell mechanics and mechanotransduction. Methods Cell Biol. 2007;83:443-72.
30. Gattazzo F, Urciuolo A, Bonaldo P. Extracellular matrix: A dynamic microenvironment for stem cell niche(). Biochim Biophys Acta. 18402014. p. 2506-19.
31. Kubow KE, Vukmirovic R, Zhe L, Klotzsch E, Smith ML, Gourdon D, et al. Mechanical forces regulate the interactions of fibronectin and collagen I in extracellular matrix. Nat Commun. 2015;6:8026.
32. Delgado O, Kaisani AA, Spinola M, Xie XJ, Batten KG, Minna JD, et al. Multipotent Capacity of Immortalized Human Bronchial Epithelial Cells. In: Parsons M, editor. PLoS One. 6. San Francisco, USA2011.
33. Kaisani A, Delgado O, Fasciani G, Kim SB, Wright WE, Minna JD, et al. Branching Morphogenesis of Immortalized Human Bronchial Epithelial Cells in Three-Dimensional Culture. Differentiation. 2014;87(0):119-26.
34. Price AP, Godin LM, Domek A, Cotter T, D'Cunha J, Taylor DA, et al. Automated Decellularization of Intact, Human-Sized Lungs for Tissue Engineering. Tissue Engineering Part C, Methods. 2015;21(1):94-103.
35. Ou K-L, Hosseinkhani H. Development of 3D in Vitro Technology for Medical Applications. International Journal of Molecular Sciences. 2014;15(10):17938-62.
36. Frangogiannis NG. Fibroblast-Extracellular Matrix Interactions in Tissue Fibrosis. Curr Pathobiol Rep. 2016;4(1):11-8.
37. Moore MW. Regulation and Relevance of Myofibroblast Responses in Idiopathic Pulmonary Fibrosis. 2013;1(3):199-208.
38. Polak J. Cell Therapy for Lung Disease. UK: Imperial College Press; 2010.
39. Crystal RG. Airway Basal Cells. The "Smoking Gun" of Chronic Obstructive Pulmonary Disease. American Journal of Respiratory and Critical Care Medicine. 2014;190(12):1355-62.
40. Humphrey JD, Dufresne ER, Schwartz MA. Mechanotransduction and extracellular matrix homeostasis. Nat Rev Mol Cell Biol. 2014;15(12):802-12.
41. Shojaie S, Ermini L, Ackerley C, Wang J, Chin S, Yeganeh B, et al. Acellular lung scaffolds direct differentiation of endoderm to functional airway epithelial cells: requirement of matrix-bound HS proteoglycans. Stem Cell Reports. 2015;4(3):419-30.
42. Waters CM, Roan E, Navajas D. Mechanobiology in Lung Epithelial Cells: Measurements, Perturbations, and Responses. Comprehensive Physiology. 2012;2(1):1-29.
43. Rosner SR, Ram-Mohan S, Paez-Cortez JR, Lavoie TL, Dowell ML, Yuan L, et al. Airway Contractility in the Precision-Cut Lung Slice after Cryopreservation. Am J Respir Cell Mol Biol. 2014;50(5):876-81.

44. Saldin LT, Cramer MC, Velankar SS, White LJ, Badylak SF. Extracellular matrix hydrogels from decellularized tissues: Structure and function. Acta Biomaterialia. 2017;49:1-15.
45. Pouliot RA. Development and Characterization of Lung Derived Extracellular Matrix Hydrogels. Richmond, Virginia: Virginia Commonwealth University.
46. Zvarova B, Uhl FE, Uriarte JJ, Borg ZD, Coffey AL, Bonenfant NR, et al. Residual Detergent Detection Method for Nondestructive Cytocompatibility Evaluation of Decellularized Whole Lung Scaffolds. Tissue Eng Part C Methods. 2016;22(5):418-28.
47. Wagner DE, Bonenfant NR, Sokocevic D, DeSarno M, Borg Z, Parsons C, et al. Three-dimensional scaffolds of acellular human and porcine lungs for high throughput studies of lung disease and regeneration. Biomaterials. 2014;35(9):2664-79.
48. Crapo PM, Gilbert TW, Badylak SF. An overview of tissue and whole organ decellularization processes. Biomaterials. 2011;32(12):3233-43.
49. Konigshoff M, Kneidinger N, Eickelberg O. TGF-beta signaling in COPD: deciphering genetic and cellular susceptibilities for future therapeutic regimen. Swiss Med Wkly. 2009;139(39-40):554-63.
50. von Haehling S, Hopkinson NS, Polkey MI, Niethammer M, Anker SD, Genth-Zotz S. Elevated TNFalpha production in whole blood in patients with severe COPD: the potential link to disease severity. Wien Klin Wochenschr. 2009;121(9-10):303-8.
51. Lee KM, Renne RA, Harbo SJ, Clark ML, Johnson RE, Gideon KM. 3-week inhalation exposure to cigarette smoke and/or lipopolysaccharide in AKR/J mice. Inhal Toxicol. 2007;19(1):23-35.
52. Tilghman RW, Cowan CR, Mih JD, Koryakina Y, Gioeli D, Slack-Davis JK, et al. Matrix Rigidity Regulates Cancer Cell Growth and Cellular Phenotype. PLoS ONE. 2010;5(9):e12905.
53. Taraseviciene-Stewart L, Douglas IS, Nana-Sinkam PS, Lee JD, Tuder RM, Nicolls MR, et al. Is alveolar destruction and emphysema in chronic obstructive pulmonary disease an immune disease? Proc Am Thorac Soc. 2006;3(8):687-90.
54. Lin CH, Yu MC, Tung WH, Chen TT, Yu CC, Weng CM, et al. Connective tissue growth factor induces collagen I expression in human lung fibroblasts through the Rac1/MLK3/JNK/AP-1 pathway. Biochim Biophys Acta. 2013;1833(12):2823-33.
55. L[ung Epithelial Biology in the Pathogenesis of Pulmonary Disease]. In: Venkataramana KS, PhD, Michael Koval P, editors.: Elsevier Academic Press; 2017.
56. Allen G, Bates JH. Dynamic mechanical consequences of deep inflation in mice depend on type and degree of lung injury. J Appl Physiol (1985). 2004;96(1):293-300.
57. Wagner DE, Fenn SL, Bonenfant NR, Marks ER, Borg Z, Saunders P, et al. Design and Synthesis of an Artificial Pulmonary Pleura for High Throughput Studies in Acellular Human Lungs. Cellular and molecular bioengineering. 2014;7(2):184-95.
58. Santoro M, Lamhamedi-Cherradi S-E, Menegaz BA, Ludwig JA, Mikos AG. Flow perfusion effects on three-dimensional culture and drug sensitivity of Ewing sarcoma. Proceedings of the National Academy of Sciences of the United States of America. 2015;112(33):10304-9.
59. Bancroft GN, Sikavitsas VI, van den Dolder J, Sheffield TL, Ambrose CG, Jansen JA, et al. Fluid flow increases mineralized matrix deposition in 3D perfusion culture of marrow stromal osteoblasts in a dose-dependent manner. Proceedings of the National Academy of Sciences of the United States of America. 2002;99(20):12600-5.
60. Wagner DE, Bonvillain RW, Jensen TJ, Girard ED, Bunnell BA, Finck CM, et al. Can Stem Cells be Used to Generate New Lungs? Ex Vivo Lung Bioengineering with Decellularized Whole Lung Scaffolds. Respirology (Carlton, Vic). 2013;18(6):10.1111/resp.12102.
61. Nelson CM, Chen CS. Cell-cell signaling by direct contact increases cell proliferation via a PI3K-dependent signal. FEBS Lett. 2002;514(2-3):238-42.
62. Bonenfant NR, Sokocevic D, Wagner DE, Borg ZD, Lathrop M, Lam YW, et al. The Effects of Storage and Sterilization on De-Cellularized and Re-Cellularized Whole Lung. Biomaterials. 2013;34(13):3231-45.
63. Jung Y, Wang J, Havens A, Sun Y, Jin T, Taichman RS. Cell-to-cell contact is critical for the survival of hematopoietic progenitor cells on osteoblasts. Cytokine. 2005;32(3-4):155-62.

64. Liu R-M. Oxidative Stress, Plasminogen Activator Inhibitor 1, and Lung Fibrosis. Antioxidants & redox signaling. 2008;10(2):303-19.
65. Waschki B, Watz H, Holz O, Magnussen H, Olejnicka B, Welte T, et al. Plasminogen activator inhibitor-1 is elevated in patients with COPD independent of metabolic and cardiovascular function. International Journal of Chronic Obstructive Pulmonary Disease. 2017;12:981-7.
66. Wei SC, Fattet L, Tsai JH, Guo Y, Pai VH, Majeski HE, et al. Matrix stiffness drives epithelial-mesenchymal transition and tumour metastasis through a TWIST1-G3BP2 mechanotransduction pathway. Nat Cell Biol. 2015;17(5):678-88.
67. Jang J-H, Chand HS, Bruse S, Doyle-Eisele M, Royer C, McDonald J, et al. Connective Tissue Growth Factor Promotes Pulmonary Epithelial Cell Senescence and Is Associated with COPD Severity. COPD: Journal of Chronic Obstructive Pulmonary Disease. 2017;14(2):228-37.
68. Shi-Wen X, Leask A, Abraham D. Regulation and function of connective tissue growth factor/CCN2 in tissue repair, scarring and fibrosis. Cytokine Growth Factor Rev. 2008;19(2):133-44.
69. Rokicki W, Rokicki M, Wojtacha J, Dżeljijli A. The role and importance of club cells (Clara cells) in the pathogenesis of some respiratory diseases. Kardiochirurgia i Torakochirurgia Polska = Polish Journal of Cardio-Thoracic Surgery. 2016;13(1):26-30.
70. Laucho-Contreras ME, Polverino F, Gupta K, Taylor KL, Kelly E, Pinto-Plata V, et al. Protective role for club cell secretory protein-16 (CC16) in the development of COPD. Eur Respir J. 2015;45(6):1544-56.
71. Zhao L, Yee M, O'Reilly MA. Transdifferentiation of alveolar epithelial type II to type I cells is controlled by opposing TGF-beta and BMP signaling. Am J Physiol Lung Cell Mol Physiol. 2013;305(6):L409-18.
72. Juan Shi FL, Meihui Luo, Jun Wei, and Xiaoming Liu. Distinct Roles of Wnt/ β -Catenin Signaling in the Pathogenesis of Chronic Obstructive Pulmonary Disease and Idiopathic Pulmonary Fibrosis,. Mediators of Inflammation. 2017;27:16.
73. Mao P, Wu S, Li J, Fu W, He W, Liu X, et al. Human alveolar epithelial type II cells in primary culture. Physiological Reports. 2015;3(2):e12288.
74. Zhang Z, Chen Z, Song Y, Zhang P, Hu J, Bai C. Expression of aquaporin 5 increases proliferation and metastasis potential of lung cancer. J Pathol. 2010;221(2):210-20.
75. Davidovich N, Chhour P, Margulies SS. Uses of Remnant Human Lung Tissue for Mechanical Stretch Studies. Cellular and molecular bioengineering. 2013;6(2):175-82.
76. Uhl F. Determination of lung regeneration using an ex vivo tissue slice model. Munich: LMU Munich; 2015.
77. Dassow C. Influence of chemical and mechanical stress on Precision-cut Lung Slices. Aachen: RWTH Aachen; 2010.
78. Ebbesson SOE. Comparative Neurology of the Telencephalon. New York: Plenum Press; 1980.